Complementary cognitive roles for D2-MSNs and D1-MSNs in interval timing

R. Austin Bruce[1], Matthew A. Weber[1], Alexandra S. Bova[1], Rachael A. Volkman[1], Casey E. Jacobs[1], Kartik Sivakumar[1], Hannah R Stutt[1], Young-cho Kim[1], Rodica Curtu[2,3], Nandakumar S. Narayanan[1,3]

[1]Department of Neurology, University of Iowa, [2]Department of Mathematics, University of Iowa, and [3]The Iowa Neuroscience Institute

***Corresponding Author**
Nandakumar Narayanan
nandakumar-narayanan@uiowa.edu
169 Newton Road
Pappajohn Biomedical Discovery Building—5336
University of Iowa, Iowa City, 52242
319-353-5698

Abstract

The role of striatal pathways in cognitive processing is unclear. We studied dorsomedial striatal cognitive processing during interval timing, an elementary cognitive task that requires mice to estimate intervals of several seconds, which involves working memory for temporal rules as well as attention to the passage of time. We harnessed optogenetic tagging to record from striatal D2-dopamine receptor-expressing medium spiny neurons (D2-MSNs) in the indirect pathway and from D1-dopamine receptor-expressing MSNs (D1-MSNs) in the direct pathway. We found that D2-MSNs and D1-MSNs exhibited opposing dynamics over temporal intervals as quantified by principal component analyses and trial-by-trial generalized linear models. MSN recordings helped construct and constrain a four-parameter drift-diffusion computational model. This model predicted that disrupting either D2-MSN or D1-MSNs would increase interval timing response times and alter MSN firing. In line with this prediction, we found that optogenetic inhibition or pharmacological disruption of either D2-MSNs or D1-MSNs increased response times. Pharmacologically disrupting D2-MSNs or D1-MSNs also increased response times, shifted MSN dynamics, and degraded trial-by-trial temporal decoding. Together, our findings demonstrate that D2-MSNs and D1-MSNs make complementary contributions to interval timing despite opposing dynamics, implying that striatal direct and indirect pathways work together to shape temporal control of action. These data provide novel insight into basal ganglia cognitive operations beyond movement and have implications for a broad range of human striatal diseases and for therapies targeting striatal pathways.

Introduction

The basal ganglia have been heavily studied in motor control (Albin et al., 1989). These subcortical nuclei are composed of two pathways defined by medium spiny neurons (MSNs) in the striatum: the indirect pathway, defined by D2-dopamine receptor-expressing MSNs (D2-MSNs) and the direct pathway, defined by D1-dopamine receptor-expressing MSNs (D1-MSNs). It has been proposed that the indirect and direct pathways play opposing roles in movement (Alexander and Crutcher, 1990; Cruz et al., 2022; Kravitz et al., 2010), although recent work identified how these pathways can play more complex and complementary roles (Cui et al., 2013; Tecuapetla et al., 2016). MSNs receive dense input from both motor and cognitive cortical areas (Averbeck et al., 2014; Graybiel, 1997; Middleton and Strick, 2000), but the respective roles of D2-MSNs and D1-MSNs in cognitive processing are largely unknown. Understanding basal ganglia cognitive processing is critical for diseases affecting the striatum such as Huntington's disease, Parkinson's disease, and schizophrenia (Andreasen, 1999; Hinton et al., 2007; Narayanan and Albin, 2022). Furthermore, pharmacological and brain stimulation therapies directly modulate D2-MSNs, D1-MSNs, and downstream basal ganglia structures such as the globus pallidus or subthalamic nucleus. Determining basal ganglia pathway dynamics cognition will help avoid side effects of current treatments and inspire novel therapeutic directions.

We studied striatal D2-MSNs and D1-MSNs during an elementary cognitive task, interval timing. This task requires estimating an interval of several seconds and provides an ideal platform to study cognition in the striatum because 1) interval timing requires cognitive resources including working memory for temporal rules and attention to the passage of time

(Parker et al., 2013); 2) it is reliably impaired in human striatal diseases such as Huntington's disease, Parkinson's disease, and schizophrenia (Merchant and de Lafuente, 2014); 3) interval timing requires nigrostriatal dopamine that modulates MSNs (Emmons et al., 2017; Gouvea et al., 2015; Matell et al., 2003; Mello et al., 2015; Monteiro et al., 2023; Wang et al., 2018); and 4) can be rigorously studied in animal models (Balci et al., 2008). Past work has shown that disrupting D2-dopamine receptors (D2s) in the dorsomedial striatum powerfully impairs interval timing (De Corte et al., 2019; Drew et al., 2007; Meck, 2006; Stutt et al., 2023). These studies have also suggested that D1-dopamine receptors (D1s) are involved in interval timing. We and others have found that striatal MSNs encode time across multiple intervals by time-dependent ramping activity, or monotonic changes in firing rate across a temporal interval (Emmons et al., 2017; Gouvea et al., 2015; Mello et al., 2015; Wang et al., 2018); however, the respective roles of D2-MSNs and D1-MSNs are unknown. Prior motor studies predict that D2-MSNs and D1-MSNs will exhibit opposing dynamics during interval timing (Alexander and Crutcher, 1990; Cruz et al., 2022; Kravitz et al., 2010; Tecuapetla et al., 2016).

We investigated dorsomedial striatal MSNs during interval timing with a combination of optogenetics, neuronal ensemble recording, computational modeling, and behavioral pharmacology. We use a well-described mouse-optimized interval timing task in which switching responses between two nosepokes reflects temporal control of action[1–4]. Strikingly, optogenetic tagging of D2-MSNs and D1-MSNs revealed that these populations have opposing neuronal dynamics, with D2-MSNs increasing firing over an interval and D1-MSNs decreasing firing over the same interval. MSN dynamics helped construct and constrain a four-parameter drift-diffusion model of interval timing. This model predicted that disrupting either D2-MSNs or D1-MSNs would increase interval timing response times. Accordingly, we found that

110 optogenetic inhibition of either D2-MSNs or D1-MSNs increased interval timing response times.
111 Furthermore, pharmacological blockade of either D2- or D1-receptors also increased response
112 times and degraded trial-by-trial temporal decoding from MSN ensembles. Thus, D2-MSNs and
113 D1-MSNs have opposing temporal dynamics yet disrupting either MSN type produced similar
114 effects on behavior. These data demonstrate that striatal pathways play complementary roles in
115 elementary cognitive operations and are highly relevant for understanding the pathophysiology
116 of human diseases and therapies targeting the striatum.

RESULTS

D2-MSNs and D1-MSNs have opposite patterns of temporal encoding.

We investigated cognitive processing in the striatum using a well described mouse-optimized interval timing task (Balci et al., 2008; Bruce et al., 2021; Larson et al., 2022; Tosun et al., 2016; Weber et al., 2023), which required mice to respond by switching between two nosepokes after an ~6 second interval (Fig 1A; see Methods). We focus on the time that mice depart the first nosepoke as the switch 'response'. Departing the first nosepoke is guided by temporal control of action because no external cue indicates when to switch from the first to the second nosepoke (Balci et al., 2008; Bruce et al., 2021; Tosun et al., 2016; Weber et al., 2023). Responses are infrequent early in the interval, peak after 6 seconds and taper off before the end of the 18-second trial, after which mice collect a 20 mg sucrose reward (data from 30 wild-type mice; response times (response time median (IQR) = 8.2 (7.2-9.8) seconds; see Table 1 for a summary of experiments; Fig 1B-C). Movement peaked before 6 seconds as animals traveled to the front nosepoke (Fig S1A-B). The first nosepokes occurred before switching responses and the second nosepokes occurred much later in the interval in anticipation of reward delivered at 18 seconds (Fig S1C-D). We studied dorsomedial striatal D2-MSNs and D1-MSNs using a combination of optogenetics and neuronal ensemble recordings in 9 transgenic mice (4 D2-Cre mice: response time 9.75 (7.02-10.35) seconds; 5 D1-Cre mice: 8.19 (7.69-8.72) seconds; rank sum $p = 0.73$; Fig 1D).

136
137

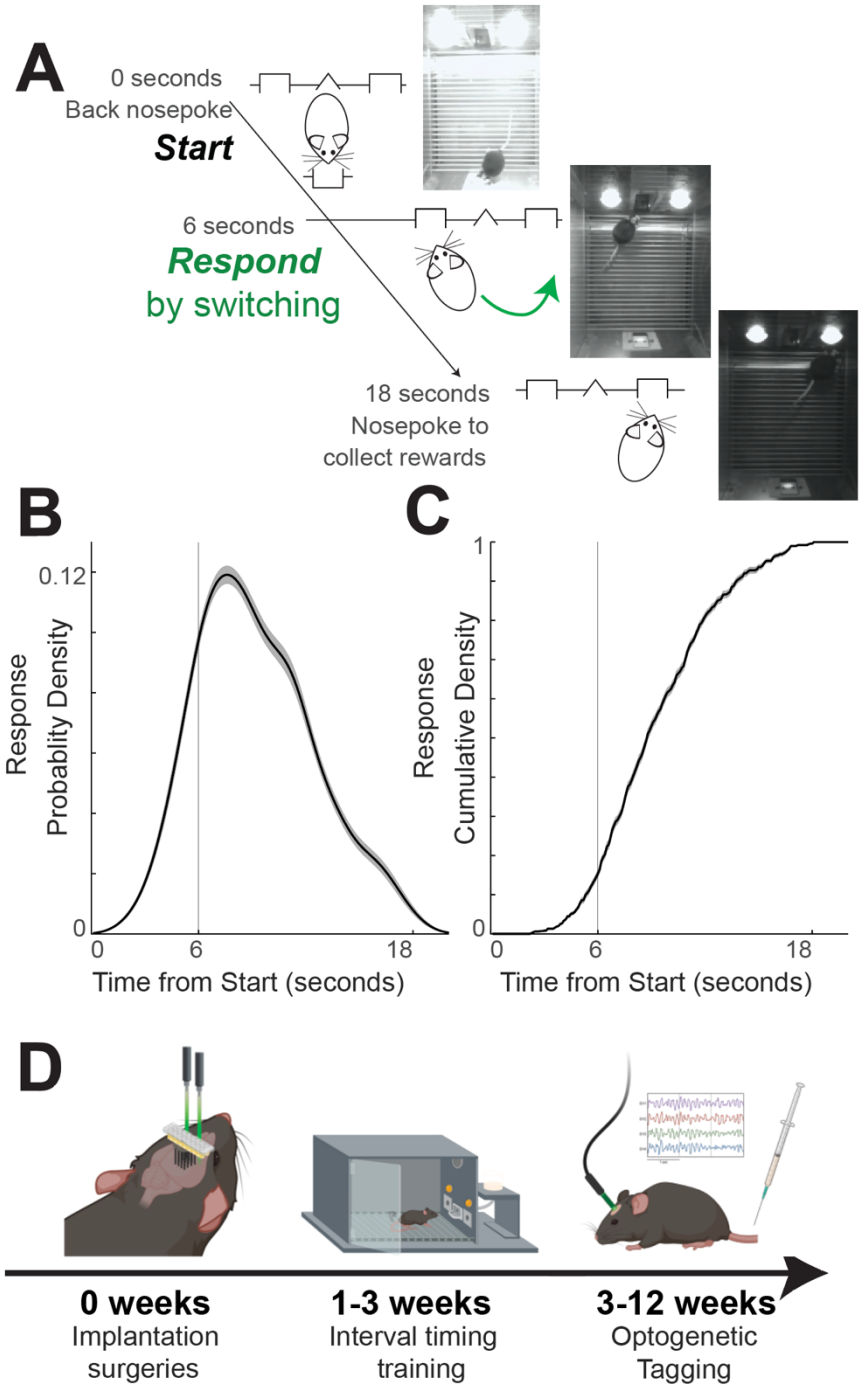

Figure 1: Mouse-optimized interval timing. A) Mice to respond by switching nosepokes after a ~6 second interval (see methods). Inset – screen captures from operant chambers. Responses to switch nosepokes are a time-based decision guided explicitly by temporal control of action (see Methods and Fig S1). Response times are defined as the moment mice exit the first nosepoke (on the left) to respond at the second nosepoke; nosepokes at a second port (on the right) after 18 seconds trigger reward delivery. B) Response probability distribution and C) cumulative density from 30 mice. D) We used optogenetic tagging to record from D2-MSNs or D1-MSNs trained to perform an interval timing task.

Striatal neuronal populations are largely composed of MSNs expressing D2-dopamine or D1-dopamine receptors. We optogenetically tagged D2-MSNs and D1-MSNs by implanting optrodes in the dorsomedial striatum and conditionally expressing channelrhodopsin (ChR2; Fig S2) in 4 D2-Cre (2 female) and 5 D1-Cre transgenic mice (2 female). This approach expressed ChR2 in D2-MSNs or D1-MSNs, respectively (Fig 2A-B; Kim et al., 2017a). We identified D2-MSNs or D1-MSNs by their spiking response to 5 millisecond pulses of 473-nm light (Fig S2B-C). We tagged 32 D2-MSNs and 41 D1-MSNs in a single recording session during interval timing (Fig 2C-F). There were no consistent differences in overall firing rate between D2-MSNs and D1-MSNs (D2-MSNs: 3.4 (1.5-7.2) Hz; D1-MSNs 5.2 (3.1-8.6) Hz; $F=2.7$, $p=0.11$ controlling for effects across individual mice). However, over the 6-second interval immediately after trial start, we discovered that D2-MSN populations appeared to ramp up (Fig 2G) while D1-MSN populations appeared to ramp down (Fig 2H). These data suggest that D2-MSNs and D1-MSNs might exhibit opposing dynamics during interval timing.

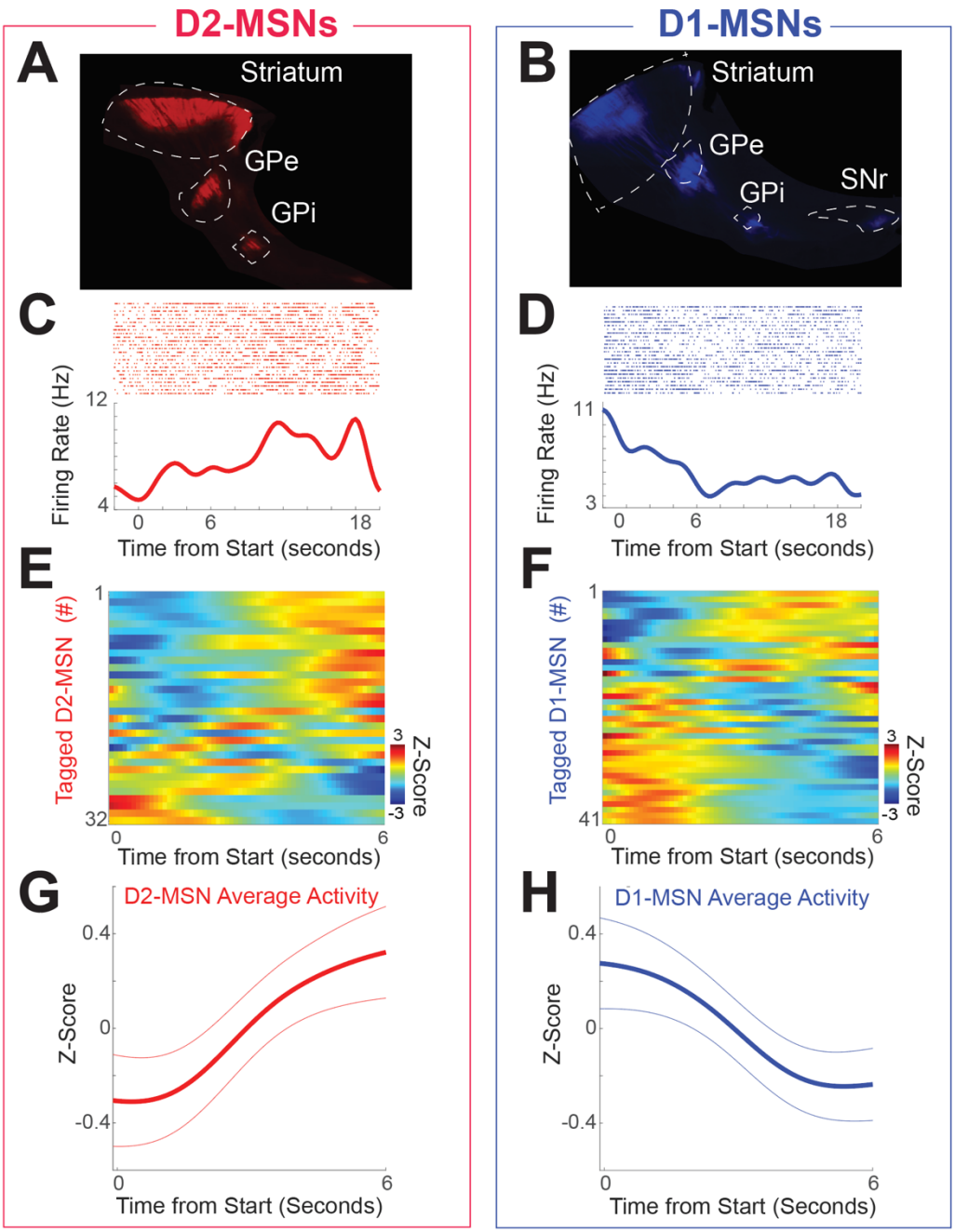

Figure 2: D2-MSNs and D1-MSNs have opposing dynamics during interval timing. A) D2-MSNs in the indirect pathway, which project from the striatum to the globus pallidus external segment (GPe; sagittal section) and internal segment (GPi) and B) D1-MSNs, which project from the striatum to the GPe, GPi, and substantia nigra (SNr; sagittal section). Peri-event raster C) from a D2-MSN (red) and E) from a D1-MSN (blue). G) Peri-event time histograms from all D2-MSNs and H) from all D1-MSNs. Average activity revealed that G) D2-MSNs (red) tended to ramp up, whereas H) D1-MSNs (blue) tended to ramp down. Data from 32 tagged D2-MSNs in 4 D2-Cre mice and 41 tagged D1-MSNs in 5 D1-Cre mice.

To quantify differences in D2-MSNs vs D1-MSNs, we turned to principal component analysis (PCA), a data-driven tool to capture the diversity of neuronal activity (Kim et al., 2017a). We analyzed MSN populations calculated from peri-event matrices from D2-MSNs and D1-MSNs over the 6-second interval immediately after trial start. PCA identified time-dependent ramping activity as PC1 (Fig 3A), a key temporal signal that explained 56% of variance among tagged MSNs (Fig 3B; Narayanan, 2016). In line with population averages from Fig 2G&H, D2-MSNs and D1-MSNs had opposite patterns of activity with negative PC1 scores for D2-MSNs and positive PC1 scores for D1-MSNs (Fig 3C; PC1 for D2-MSNs: -5.1 (-6.4–3.4); PC1 for D1-MSNs: 4.21 (-4.5–6.9); F=8.7, p = 0.004 controlling for effects across individual mice; Cohen's d = 0.7; no reliable effect of sex (p=0.81) or switching direction (p=0.36)). Thus, PCA analyses also showed that D2-MSN populations ramped up, while D1-MSN populations ramped down.

To interrogate these dynamics at a trial-by-trial level, we calculated the linear slope of D2-MSN and D1-MSN activity over the first 6 seconds of each trial using generalized linear modeling (GLM) of trial-by-trial firing rate (Latimer et al., 2015). Nosepokes were included as a regressor for movement. GLM analysis also demonstrated that D2-MSNs had a positive linear slope of firing rate vs time in the interval (0.02 spikes/second (-0.07–0.21)), implying that D2-MSNs ramped up compared to D1-MSNs, which ramped down (Fig 3D; negative linear slope of -0.14 spikes/second (-0.35–0.01); F=5.6, p = 0.04 controlling for effects across individual mice; Cohen's d = 0.7; no reliable effect of sex (p=0.18) or switching direction (p=0.41)). These findings are in line with population averages in Fig 2G&H as well as PCA results in Fig 3A-C, and could not be fully explained by movement because 1) few responses occurred before 6 seconds (23%) and 44% of tagged neurons were recorded in sessions without a single nosepoke before 6 seconds (Fig 1B-C), 2) our GLM included a regressor accounting for the nosepokes

when present, and 3) nosepoke GLM βs were not reliably different between D2-MSNs and D1-MSNs (rank sum $p = 0.61$). Furthermore, differences between D2-MSNs and D1-MSNs were consistent over the entire 0–18 second interval (Fig S3). Together, these data provide convergent evidence that D2-MSNs and D1-MSNs had opposing dynamics during the interval timing task.

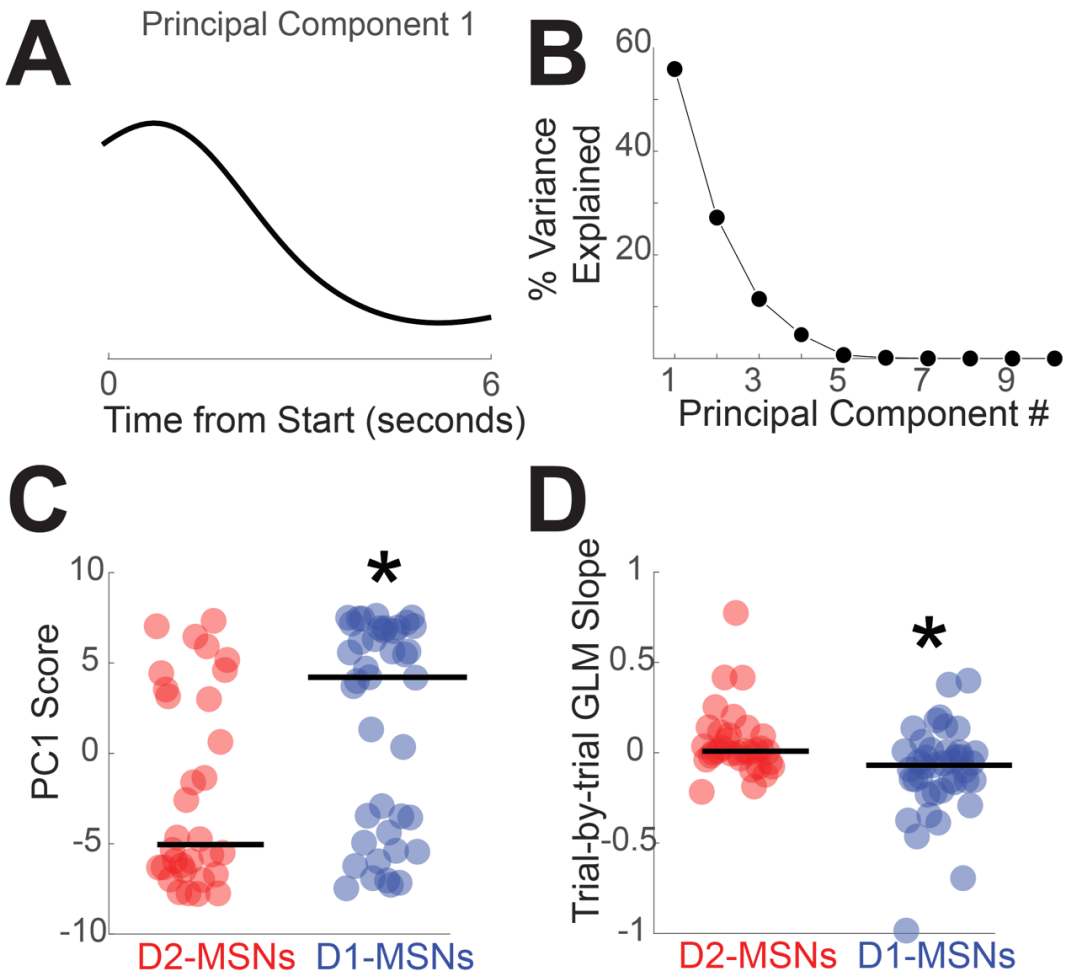

Figure 3: Quantification of opposing D2-MSN and D1-MSN dynamics A) Principal component analysis revealed that the first component (PC1) exhibited time-dependent ramping. B) The first principal component explained ~56% of variance across tagged MSN ensembles. C) Differences between D2-MSNs (red) and D1-MSNs (blue) were captured by PC1 which exhibited time-dependent ramping. D) These differences were also apparent in the linear slope of firing rate vs time in the interval, with D1-MSNs (blue) having a more negative slope than D2-MSNs (red). The differences were unlikely to be driven by movement because most responses occur after 6 seconds, our GLMs included nosepokes as a regressor, and nosepoke GLM βs were similar between D2-MSNs and D1-MSNs. In C and D, each point represents data from a tagged MSN, and horizontal black lines represent group medians. * $p < 0.05$ via linear mixed effects models accounting individual mice. Data from 32 tagged D2-MSNs in 4 D2-Cre mice and 41 tagged D1-MSNs in 5 D1-Cre mice.

Striatal MSNs can predict response times during interval timing (Gouvea et al., 2015; Mello et al., 2015). We examined how D2-MSNs and D1-MSNs predicted response times during our task. For each mouse, we divided response times into tertiles. Then, we used MSN ensembles to predict response time tertiles using neural network-based machine-learning classifiers. We found that response time predictions did not reliably differ between D2-MSN ensembles and D1-MSN ensembles (classifier prediction accuracy from D2-MSN ensembles: 38% (32%-42%); from D1-MSN ensembles: 38% (30%-56%); rank sum $p = 0.68$).

In summary, we used optogenetic tagging to record from D2-MSNs and D1-MSNs during interval timing. Although MSN activity is diverse (Fig 2E-F), linear differences both in slope and PC1 captured differences between D2-MSNs and D1-MSNs, suggesting that D2 MSNs and D1-MSNs had opposing dynamics during interval timing. These data provide insight into temporal processing by striatal MSNs.

Drift-diffusion models of opposing D2-MSN and D1-MSN dynamics.

Our data demonstrate that D2-MSNs and D1-MSNs have opposite activity patterns. However, past computational models of interval timing have relied on drift-diffusion dynamics with a positive slope that accumulates evidence over time (Nguyen et al., 2020; Simen et al., 2011). To reconcile how these MSNs might complement to effect temporal control of action, we constructed a four-parameter drift-diffusion model (DDM), where x represents the neuronal firing rate, t represents time measured in seconds, and dx and dt mean "change" in x and t respectively (equivalent to the derivative dx/dt):

$$dx = (F - x)Ddt + \sigma d\xi(t) \qquad \text{(Equation 1)}$$

$$x(0) = b \qquad \text{(Equation 2)}$$

The model has four independent parameters $F, D, \sigma,$ and b (described below) and a threshold value T defined by

$$T = T(F, b) = \left(1 - \frac{1}{4}b\right)F + \frac{1}{4}b(1 - F) \qquad \text{(Equation 3)}$$

The firing rate is set initially at baseline b (see Equation 2), then driven by input F akin to the dendritic current induced by the overlap of corticostriatal postsynaptic potentials (Shepherd, 2013). With each unit of time *dt*, we suppose there is corticostriatal stimulation that provides incremental input proportional to the activity itself, $(F - x)D$, to reach a decision. D is *the drift rate* for the event sequence and can be interpreted as a parameter inverse proportional to the neural activity's integration time constant. The drift, together with noise $\xi(t)$ (of zero mean and strength σ), leads to fluctuating accumulation which eventually crosses a threshold T (see Equation 3; Fig 4A-B). The time t^* it takes the firing rate to reach the threshold, $x(t^*) = T$, is the *response time*.

This instantiation of DDMs captured the complimentary D2-MSN and D1-MSN dynamics that we discovered in our optogenetic tagging experiments (Fig 2G-H vs. 4A-B). The model's parameters were chosen as: $F = 1,\ b = 0.52$ (so $T = 0.87$), $D = 0.135,\ \sigma = 0.053$ for intact D2-MSNs (Fig 4A, in black); and $F = 0, b = 0.48$ (so $T = 0.12$), $D = 0.141,\ \sigma = 0.053$ for intact D1-MSNs (Fig 4B, in black). Interestingly, we observed that two-parameter gamma distributions almost perfectly accounted for the model dynamics (D2-MSNs: Gamma parameters $\alpha = 6.08$, $\beta = 0.69$, R^2 vs Model = 0.99; D1-MSNs $\alpha = 5.89$, $\beta = 0.69$; R^2 vs Model = 0.99; Fig 2C-D, dotted black lines). Gamma distributions provided a surprisingly good approximation for the probability distribution and cumulative distribution functions of mouse response times (Fig

1B-C). Thus, in the next sections, we used gamma distributions as a proxy for both the distribution of times generated by the model and the distribution of mice response times, when comparing those for the goodness of fit.

Our model provided the opportunity to computationally explore the consequences of disrupting D2-MSNs or D1-MSNs. Because both D2-MSNs and D1-MSNs accumulate temporal evidence, disrupting either MSN type in the model changed the slope. The results were obtained by simultaneously decreasing the drift rate D (equivalent to lengthening the neurons' integration time constant) and lowering the level of network noise σ: $D = 0.129, \sigma = 0.044$ for D2-MSNs in Fig 4A (in red); and $D = 0.122, \sigma = 0.044$ for D1-MSNs in Fig 4B (in blue). The model predicted that disrupting either D2-MSNs or D1-MSNs would increase response times (Fig 4C and Fig 4D) and would shift MSN dynamics. In the next section, we interrogated these ideas with a combination of optogenetics, behavioral pharmacology, and electrophysiology.

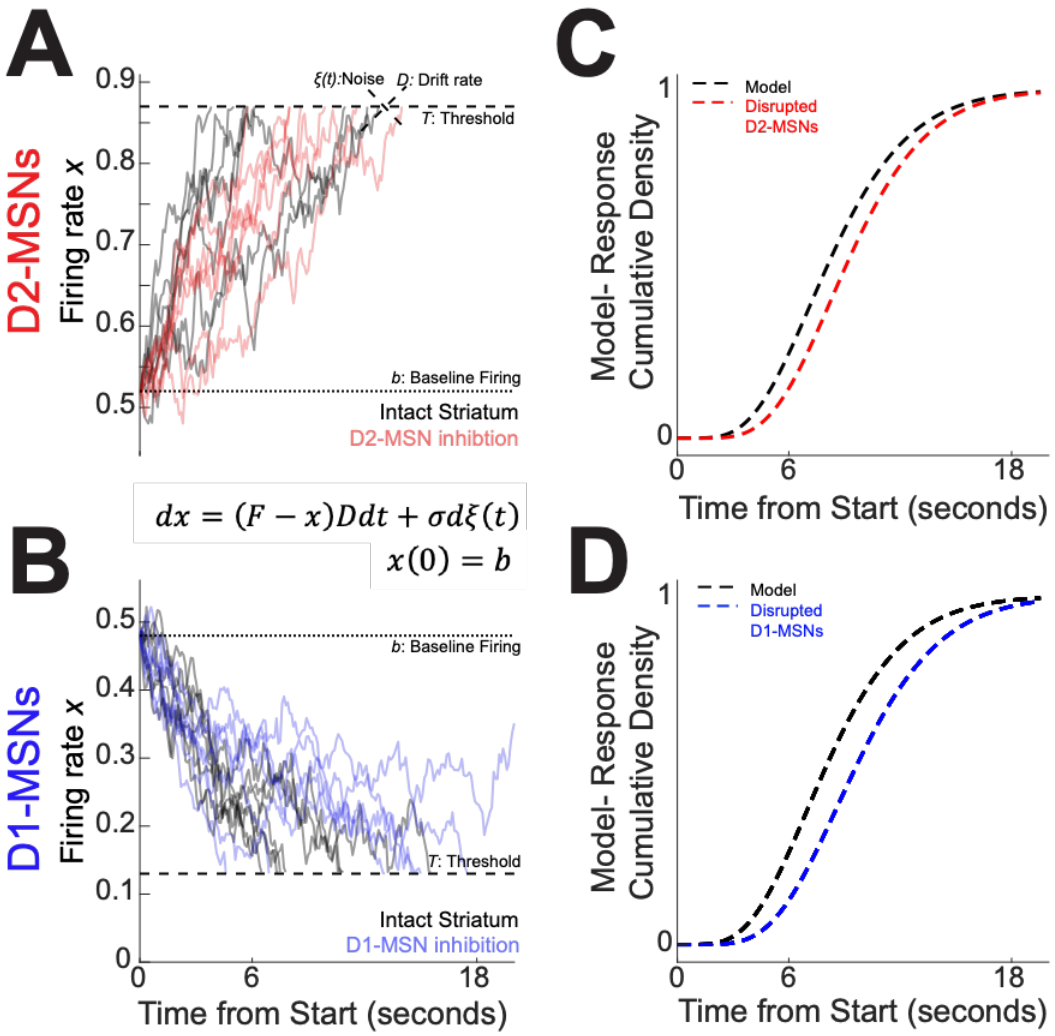

Figure 4: Four-parameter drift-diffusion computational model of striatal activity during interval timing. A) We modeled interval timing with a low parameter diffusion process with a drift rate *D*, noise $\xi(t)$, and a baseline firing rate *b* that drifts toward a threshold *T* indicated by dotted lines. With D2-MSNs disrupted (solid red curves), this drift process decreases in slope and takes longer to reach the threshold. B) The same model also accounted for D1-MSNs that had an opposite drift slope. With D1-MSNs disrupted (solid blue curves), the drift process again takes longer to reach the threshold. Because both D2-MSNs and D1-MSNs contribute to the accumulation of temporal evidence, this model predicted that C) disrupting D2-MSNs would increase response times during interval timing (dotted red line) and D) disrupting D1-MSNs would also increase response times (dotted blue line). Threshold *T* depends on *b* and target firing *F*.

251 ***Disrupting D2-MSNs or D1-MSNs increases response times.***

252 DDMs captured opposing MSN dynamics and predicted that disrupting either D2-MSNs
253 or D1-MSNs should slow temporal processing and increase response times (Fig 4). We tested
254 this idea with optogenetics. We bilaterally implanted fiber optics and virally expressed the
255 inhibitory opsin halorhodopsin in the dorsomedial striatum of 10 D2-Cre mice (5 female) to
256 inhibit D2-MSNs (Fig S4; this group of mice was entirely separate from the optogenetic tagging
257 mice). We found that D2-MSN inhibition reliably increased response times (Fig 5A-B; Laser
258 Off: 8.6 seconds (8.3–9.3); Laser On: 10.2 seconds (9.4–10.2); signed rank $p = 0.002$, Cohen's d
259 $= 1.7$; no effect in no-opsin controls; Fig S5). Remarkably, DDMs predictions were highly
260 concordant with D2-MSN inhibition behavioral data ($R^2 = 0.55$) as well as with behavioral data
261 from laser off trials ($R^2 = 0.63$; Fig S6).

262 Next, we investigated D1-MSNs (Kravitz et al., 2010). In 6 D1-Cre mice (3 female),
263 optogenetic inhibition of dorsomedial striatal D1-MSNs increased response times (Fig 5C-D;
264 Laser Off: 8.7 (8.0–9.1) seconds; Laser On: 10.5 (9.6–11.1) seconds; signed rank $p = 0.03$,
265 Cohen's $d = 1.4$; no effect in no-opsin controls; Fig S5). DDM predictions again were highly
266 concordant with D1-MSN inhibition behavioral data ($R^2 = 0.56$) and with laser off trials ($R^2 =$
267 0.64; Fig S6).

268 To test the generality of the effects observed in the optogenetic inhibition experiment, we
269 turned to systemic pharmacology. We used sulpiride (12.5 mg/kg intraperitoneally (IP)) to block
270 D2-dopamine receptors in 10 wild-type (WT) mice, which increased response times relative to
271 saline sessions (median (IQR); saline: 8.9 (8.4-9.8) seconds; D2 blockade: 10.1 (9.4-10.8)
272 seconds; signed rank $p = 0.002$, Cohen's $d = 1.0$; Fig 5E-F; Stutt et al., 2023). Of note, there was
273 no difference in response time between saline sessions and laser off trials from D2-MSN

optogenetic inhibition in D2-Cre mice, implying that in optogenetic sessions, D2-MSN inhibition did not disrupt behavior during laser off trials (rank sum $p = 0.31$). These data are consistent with past work demonstrating that disrupting dorsomedial D2-MSNs slows timing (De Corte et al., 2019; Drew et al., 2007; Stutt et al., 2023). In the same 10 wild-type mice, systemic drugs blocking D1-dopamine receptors (D1 blockade; SCH23390 0.05 mg/kg IP) increased response times (saline: 9.7 seconds (9.0-9.9); D1 blockade: 10.1 seconds (9.3-11.4); signed rank $p = 0.04$, Cohen $d = 0.7$; Fig 5G-H). Once again, there was no difference between saline sessions and D1-MSN inhibition laser off trials in D1-Cre mice (rank sum $p = 0.18$). These results are in line with our DDM predictions and demonstrate that disrupting either D2-MSNs or D1-MSNs increases response time.

We found no evidence that inhibiting D2-MSNs in the dorsomedial striatum changed task-specific movements such as nosepoke duration (i.e., time of nosepoke entry to exit; signed rank $p = 0.63$; Fig S7 for the 10 D2-Cre mice in optogenetics trials) or switch traversal time between the first and second nosepokes (signed rank $p = 0.49$; Fig S7). Similarly, we found no evidence that D1-MSN inhibition changed nosepoke duration (signed rank $p = 0.31$; Fig S7 for the 6 D1-Cre mice) or traversal time (signed rank $p = 0.22$; Fig S7). Furthermore, disrupting D2-MSNs or D1-MSNs did not change response time standard deviations or the number of rewards (Fig S8). These results demonstrate that disrupting dorsomedial striatal D2-MSNs and D1-MSNs specifically slowed interval timing without consistently changing task-specific movements.

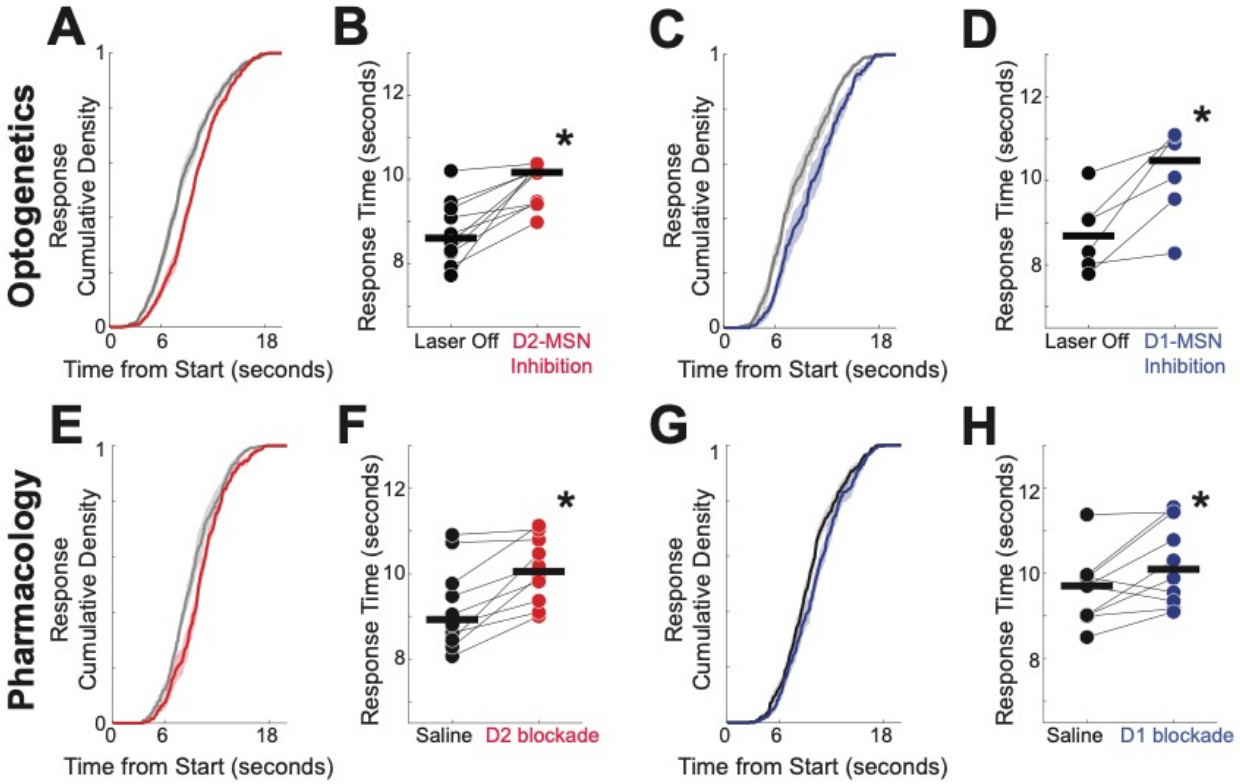

Figure 5: Disrupting D2- or D1-MSNs increases response times. A) As predicted by our DDM in Fig 4, optogenetic inhibition of D2-MSNs (red) shifted cumulative distributions of response times to the right, and B) increased response times; data from 10 D2-Cre mice expressing halorhodopsin (Halo). Also as predicted by our DDM, optogenetic inhibition of D1-MSNs C) shifted cumulative distribution functions to the right, and D) increased response times; data from 6 D1-Cre mice expressing Halo. Similarly, E) pharmacologically disrupting D2-dopamine receptors (red) with the D2 antagonist sulpiride shifted cumulative distribution functions to the right, and F) increased response times; data from 10 wild-type mice. Also, G) pharmacologically disrupting D1-dopamine receptors (blue) with the D1 antagonist SCH23390 shifted cumulative distribution functions to the right, and H) increased response times; data from the same 10 wild-type mice as in E-F. In B, D, F, and H connected points represent the mean response time from each animal in each session, and horizontal black lines represent group medians. *$p = < 0.05$, signed rank test.

297

298

299

300 ***D2 blockade and D1 blockade shifts MSN dynamics and degrades MSN temporal encoding.***

301 MSN ensembles strongly encode time (Bruce et al., 2021; Emmons et al., 2017; Gouvea
302 et al., 2015; Mello et al., 2015; Wang et al., 2018), but it is unknown how disruptions in D2-
303 dopamine or D1-dopamine receptors affect these ensembles (Yun et al., 2023). Although non-
304 specific, pharmacological experiments have two advantages over optogenetics for recording
305 experiments: 1) many clinically approved drugs target dopamine receptors, and 2) they are more
306 readily combined with recordings than optogenetic inhibition, which silences large populations
307 of MSNs. We recorded from dorsomedial striatal MSN ensembles in 11 separate mice during
308 sessions with saline, D2 blockade with sulpiride, or D1 blockade with SCH23390 (Fig 6A; Fig
309 S2; data from one recording session each for saline, D2 blockade, and D1 blockade during
310 interval timing).

311 We analyzed MSN ensembles in sessions with saline (158 neurons), D2 blockade (167
312 neurons), or D1 blockade (144 neurons; Fig 6B-C). There were no consistent changes in MSN
313 firing rate with D2 blockade or D1 blockade ($F=2.0$, $p=0.13$ controlling for effects across
314 individual mice; saline: 4.8 (3.2-8.3) Hz; D2 blockade 4.8 (2.3-7.6) Hz)); D1 blockade (4.1 (2.3-
315 7.1) Hz), suggesting that blocking D2 or D1 dopamine receptors may have complex effects on
316 dorsomedial striatal MSNs (Kreitzer, 2009). We used PCA to analyze these dynamics during
317 interval timing (Bruce et al., 2021; Emmons et al., 2017; Kim et al., 2017a). Population analyses
318 were performed by constructing principal components (PC) from z-scored peri-event time
319 histograms of firing rate from saline, D2 blockade, and D1 blockade sessions together (Fig 6D-E;
320 Fig S9 for analysis of the same neurons across sessions). Examination of the individual
321 components revealed that the first component (PC1), which explained 55% of neuronal variance,
322 exhibited "time-dependent ramping", or monotonic changes over the 6 second interval

immediately after trial start (Fig 6D-E). Because PC1 scores can either be positive or negative, this metric likely represented changes in the drift rate from our DDMs.

Interestingly, PC1 scores shifted with dopaminergic blockade (F = 3.3, p = 0.04 controlling for effects across individual mice; no reliable effect of sex (p=0.58) or switching direction (p=0.58); D2 blockade: (0.7 (-6.4–5.1) vs saline: 3.7 (-4.4–5.8), post-hoc p = 0.02; D1 blockade (0.7 (-6.7–5.2), post-hoc vs saline p = 0.03; Fig 6F). The second component (PC2) explained 31% of the variance (Fig 6D-E), and few reliable differences were found in PC2 or higher components (Fig 6G). This data-driven analysis shows that D2 and D1 blockade produced similar shifts in MSN population dynamics represented by PC1. As with our tagging data in Figure 3, it is remarkable that despite MSN diversity (Fig 6C) linear dynamics captured by PC1 shift with D2 and D1 blockade; deeper analyses are detailed in Fig S9. The decrease in PC1 scores of the MSN neuronal ensemble observed during the pharmacological blockade (Fig 6F) is in line with predictions made by our DDM, which simulated delayed response times in MSN inhibition by lowering the drift rate (Fig 2).

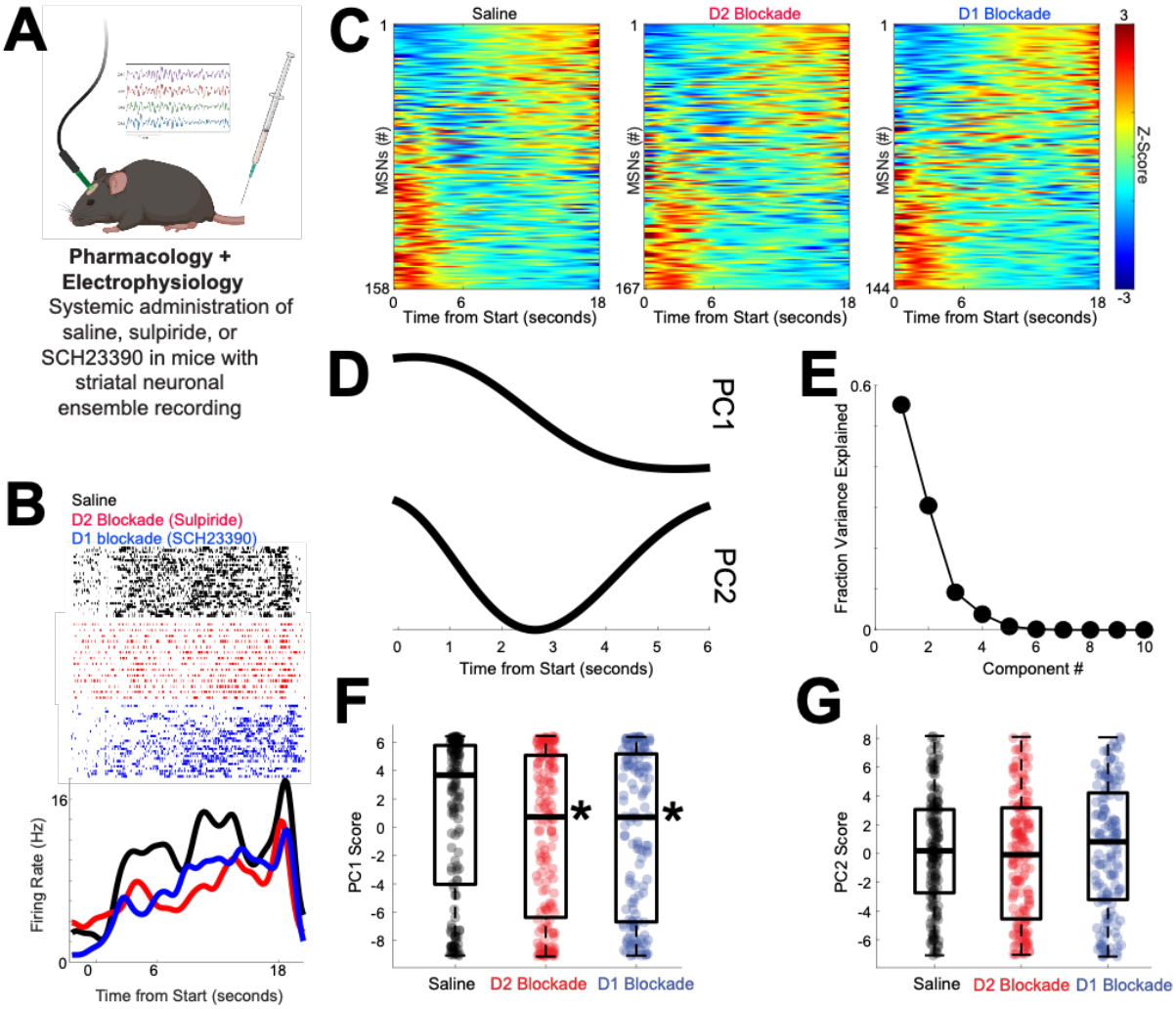

Figure 6: D2 and D1 blockade shift temporal dynamics. A) We recorded dorsomedial striatal medium spiny neuron (MSN) ensembles during interval timing in sessions with saline, D2 blockade with sulpiride, or D1 blockade with SCH23390. Made with BioRender.com. B) Peri-event raster from a single MSN in sessions with saline (black), D2-dopamine blockade (red), or D1-dopamine blockade (blue). D2 blockade or D1 blockade changed this MSN's temporal dynamics. C) Neuronal ensemble recording from the same 11 animals with saline, D2 blockade, or D1 blockade; each row represents a peri-event time histogram. Colors indicate z-scored firing rate. D) Principal component analysis (PCA) identified MSN ensemble patterns of activity. The first principal component (PC1) exhibited time-dependent ramping. E) PC1 explained 55% of population variance among MSN ensembles; the second principal component (PC2) explained 31%; higher components explained <10% each and were not analyzed. F) PC1 scores were shifted and significantly different with D2 or D1 blockade, but G) PC2 scores were not. *$p < 0.05$ via linear mixed effect models; data from 11 mice.

338

339 Finally, we quantified striatal MSN temporal encoding via a naïve Bayesian classifier
340 that generates trial-by-trial predictions of time from MSN ensemble firing rates (Fig 7A-C;
341 Bruce et al., 2021; Emmons et al., 2017). Our DDMs predict that disrupted temporal decoding
342 would be a consequence of an altered DDM drift rate. We used leave-one-out cross-validation to
343 predict objective time from the firing rate within a trial. Saline sessions generated strong
344 temporal predictions for the first 6 seconds of the interval immediately after trial start (0–6
345 seconds; $R^2 = 0.91$ (0.83–0.94)) with weaker predictions for later epochs (6–12 seconds: $R^2 =$
346 0.55 (0.33–0.70); rank sum $p = 0.00002$ vs 0–6 seconds, Cohen $d = 2.1$; 12–18 seconds: $R^2 =$
347 0.16 (0.08–0.64); rank sum $p = 0.00005$ vs 0–6 seconds, Cohen $d = 2.3$; analyses considered
348 statistically independent; Fig 7D). We found that temporal encoding early in the interval (0–6
349 seconds) was degraded with either D2 blockade ($R^2 = 0.69$ (0.59–0.84); rank sum $p = 0.0003$ vs
350 saline, Cohen $d = 1.4$) or D1 blockade ($R^2 = 0.70$ (0.47–0.87); rank sum $p = 0.006$ vs saline,
351 Cohen $d = 1.2$; Fig 7D), in line with predictions made from DDMs. Later in the interval (6–12
352 and 12-18 seconds), there were no significant differences between saline sessions and D2
353 blockade or D1 blockade (Fig 7D). Disrupting either D2-MSNs or D1-MSNs degraded MSN
354 temporal encoding.
355 We compared machine-learning predictions of response time tertiles using neural
356 network-based classifiers between saline, D2 blockade, and D1 blockade sessions. We found few
357 reliable differences between saline (35% (27%-43%)), D2 blockade (43% (35%-50%; signed
358 rank $p = 0.76$ vs saline), and D1 blockade (52% (24%-54%); signed rank $p = 0.32$ vs saline;
359 signed rank $p = 0.12$ vs D2 blockade). As with our earlier analyses of tagged D2-MSN and D1-
360 MSN ensembles, these data show that MSNs marginally predict response time over chance
361 (33%), and these predictions were not reliably affected by D2 or D1 blockade. Taken together,

these data demonstrate that disrupting D2-MSNs or D1-MSNs degrades temporal encoding by MSN ensembles. In combination with our optogenetic tagging, computational modeling, and optogenetic inhibition experiments, these data provide insight into cognitive computations by the striatum.

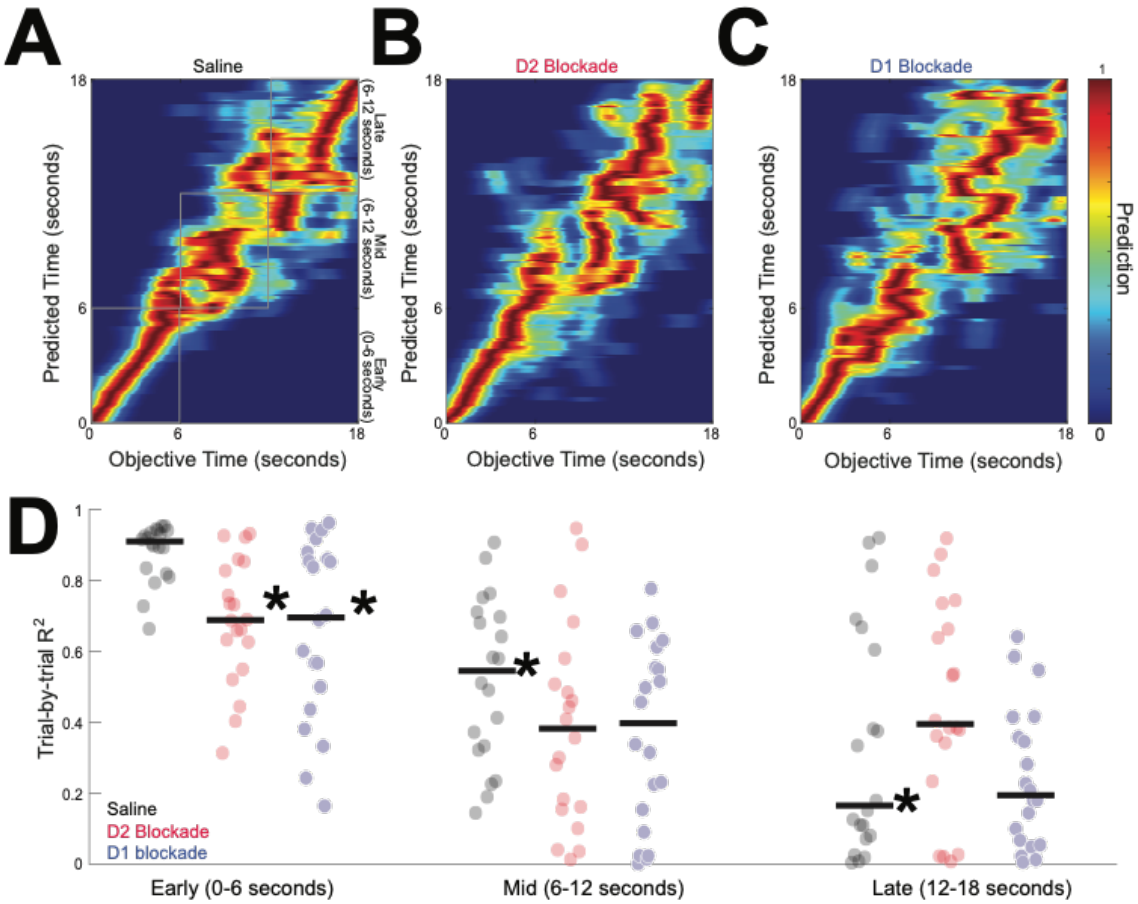

Figure 7: D2 and D1 blockade degrade MSN temporal encoding. We used naïve Bayesian classifiers to decode time from MSN ensembles in A) saline sessions, B) D2 blockade sessions, and C) D1 blockade sessions. Color represents the temporal prediction across 20 trials with red representing stronger predictions. D) Temporal encoding was strong early in the interval, and D2 or D1 blockade degraded classification accuracy. Temporal encoding was decreased later in the interval. Each point represents the R^2 for each trial of behavior for MSN ensembles from 11 mice. * $p < 0.05$ vs saline from 0-6 seconds. Horizontal black lines in (D) represent group medians.

370 **DISCUSSION**

371

372 We describe how striatal MSNs work together in complementary ways to encode an
373 elementary cognitive process, interval timing. Strikingly, optogenetic tagging showed that D2-
374 MSNs and D1-MSNs had opposing patterns of activity with D2-MSNs ramping up over the
375 interval and D1-MSNs ramping down. MSN dynamics helped construct and constrain a four-
376 parameter drift-diffusion model in which D2- and D1-MSN spiking accumulated temporal
377 evidence. This model predicted that disrupting either D2-MSNs or D1-MSNs would increase
378 response times. Accordingly, we found that optogenetically or pharmacologically disrupting
379 striatal D2-MSNs or D1-MSNs increased response times without affecting task-specific
380 movements. Disrupting D2-MSNs or D1-MSNs shifted MSN temporal dynamics and degraded
381 MSN temporal encoding. These data, when combined with our model predictions, demonstrate
382 that D2-MSNs and D1-MSNs contribute temporal evidence to controlling actions in time. Our
383 results provide new insight into how opposing patterns of striatal MSN activity control behavior
384 in similar ways and show that they play a complementary role in elementary cognitive
385 operations.

386 Striatal MSNs are critical for temporal control of action (Emmons et al., 2017; Gouvea et
387 al., 2015; Mello et al., 2015). Three broad models have been proposed for how striatal MSN
388 ensembles represent time: 1) the striatal beat frequency model, in which MSNs encode temporal
389 information based on neuronal synchrony (Matell and Meck, 2004); 2) the distributed coding
390 model, in which time is represented by the state of the network(Paton and Buonomano, 2018);
391 and 3) the DDM, in which neuronal activity monotonically drifts toward a threshold after which
392 responses are initiated (Emmons et al., 2017; Simen et al., 2011; Wang et al., 2018). While our
393 data do not formally resolve these possibilities, our results show that D2-MSN and D1-MSNs

394 exhibit opposing linear changes in firing rate dynamics in PC1 over the interval. Past work by
395 our group and others have demonstrates that these linear dynamics can scale over multiple
396 intervals to represent time (Emmons et al., 2020, 2017; Gouvea et al., 2015; Mello et al., 2015;
397 Wang et al., 2018). We find that low-parameter DDMs account for interval timing behavior with
398 both intact and disrupted striatal D2- and D1-MSNs. While other models can capture interval
399 timing behavior and account for MSN neuronal activity, our model does so parsimoniously with
400 relatively few parameters (Matell and Meck, 2004; Paton and Buonomano, 2018; Simen et al.,
401 2011). We and others have shown previously that ramping activity scales to multiple intervals,
402 and DDMs can be readily adapted by changing the drift rate (Emmons et al., 2017; Gouvea et al.,
403 2015; Mello et al., 2015; Simen et al., 2011). Interestingly, decoding performance was high early
404 in the interval; indeed, animals may have been focused on this initial interval (Balci and
405 Gallistel, 2006) in making temporal comparisons and deciding whether to switch response
406 nosepokes.

407 D2-MSNs and D1-MSNs play complementary roles in movement. For instance,
408 stimulating D1-MSNs facilitates movement, whereas stimulating D2-MSNs impairs movement
409 (Kravitz et al., 2010). Both populations have been shown to have complementary patterns of
410 activity during movements (Tecuapetla et al., 2016), with MSNs firing at different phases of
411 action initiation and selection. Further dissection of action selection programs reveals that
412 opposing patterns of activation among D2-MSNs and D1-MSNs suppress and guide actions,
413 respectively, in the dorsolateral striatum (Cruz et al., 2022). A particular advantage of interval
414 timing is that it captures a cognitive behavior within a single dimension — time. When projected
415 along the temporal dimension, it is surprising that D2-MSNs and D1-MSNs have opposing
416 patterns of activity. Past work from our group and others have shown that disrupting D2 or D1

417 MSNs slows timing (De Corte et al., 2019; Drew et al., 2007, 2003; Stutt et al., 2023).
418 Computational modeling predicted that disrupting either D2-MSNs or D1-MSNs increased self-
419 reported estimates of time, which was supported by both optogenetic and pharmacological
420 experiments. Notably, these disruptions are distinct from increased timing variability reported
421 with administrations of amphetamine, ventral tegmental area dopamine neuron lesions, and
422 rodent models of neurodegenerative disease (Balci et al., 2008; Gür et al., 2020, 2019; Larson et
423 al., 2022; Weber et al., 2023). \Furthermore, our current data demonstrate that disrupting either
424 D2-MSN or D1-MSN activity shifted MSN dynamics and degraded temporal encoding,
425 supporting prior work (De Corte et al., 2019; Drew et al., 2007, 2003; Stutt et al., 2023). Our
426 recording experiments do not identify where a possible response threshold *T* is instantiated, but
427 downstream basal ganglia structures may have a key role in setting response thresholds (Toda et
428 al., 2017).

429 Since interval timing is reliably disrupted in human diseases of the striatum such as
430 Huntington's disease, Parkinson's disease, and schizophrenia (Hinton et al., 2007; Singh et al.,
431 2021; Ward et al., 2011), these results have relevance to human disease. Furthermore, because
432 many therapeutics targeting dopamine receptors are used clinically, our findings illuminate how
433 dopaminergic drugs affect cognitive function and dysfunction. Finally, D2-MSNs and D1-MSNs
434 define indirect and direct pathways, which are targeted by deep brain stimulation for
435 neurological and psychiatric disease.

436 Our approach has several limitations. First, systemic drug injections block D2- and D1-
437 receptors in many different brain regions, including the frontal cortex, which is involved in
438 interval timing (Kim et al., 2017a). D2 blockade or D1 blockade may have complex effects,
439 including corticostriatal or network effects that contribute to changes in D2-MSN or D1-MSN

ensemble activity. Despite these limitations, pharmacology is compatible with neuronal ensemble recordings, whereas optogenetic inhibition would silence a large fraction of neurons, complicating interpretations. Second, optogenetic tagging is low-yield, and it is possible that recording more of these neurons would afford greater opportunity to identify alternative coding schemes, such as neuronal synchrony. Larger neuronal ensembles might improve prediction of response times, although we note that it is remarkable that MSNs strongly predicted time but marginally predicted responses. Third, the striatum includes diverse cell types, some of which express D1 and D2 dopamine receptors and these cell types may also contribute to cognitive processing. Fourth, MSNs can laterally inhibit each other, which may profoundly affect striatal function. Regardless, we show that cell-type-specific disruption of D2-MSNs and D1-MSNs both slow timing, implying that these cell types play a key role in interval timing, and our optogenetic tagging experiments describe their activity at high temporal resolution. Future experiments may record from non-MSN striatal cell types, including fast-spiking interneurons that shape basal ganglia output. Fifth, there may be key anatomic differences between dorsal striatal regions that we did not capture (Gerfen, 1984). Sixth, we did not deliver stimulation to the striatum, because our pilot experiments triggered movement artifacts or task-specific dyskinesias (Kravitz et al., 2010). Future stimulation approaches carefully titrated to striatal physiology may affect interval timing without affecting movement. Finally, movement and motivation contributes to MSN dynamics (Robbe, 2023). Importantly, three lines of evidence argue that our findings cannot be directly explained by motor confounds: 1) D2-MSNs and D1-MSNs diverge early in the interval well before the first nosepoke, 2) our GLM accounted for nosepokes and nosepoke-related βs were similar between D2-MSNs and D1-MSNs, 3) optogenetic disruption of dorsomedial D2-MSNs and D1-MSNs did not change task-specific

463 movements despite reliable changes in response time, and 4) ramping dynamics were quite
464 distinct from movement dynamics. Furthermore, disrupting D2-MSNs and D1-MSNs did not
465 change the number of rewards animals received, implying that these disruptions did not grossly
466 affect motivation. Still, future work combining motion tracking with neuronal ensemble
467 recording and optogenetics in the context of a bisection task may further unravel timing vs.
468 movement in MSN dynamics (Robbe, 2023). Finally, the Cre lines used here may involve off-
469 target expression, particularly in the case of D2-Cre mice, although our spike-sorting criteria was
470 chosen to identify MSNs (Bruce et al., 2021; Emmons et al., 2017).

471 In summary, we examined the role of dorsomedial striatal D2-MSNs and D1-MSNs
472 during an elementary cognitive behavior, interval timing. Optogenetic tagging revealed that D2-
473 MSNs and D1-MSNs exhibited opposite and complementary patterns of neuronal activity. These
474 dynamics could be captured by computational drift-diffusion models, which predicted that
475 disrupting either D2-MSNs or D1-MSNs would slow the accumulation of temporal evidence and
476 increase response time. In line with this prediction, we found that optogenetic or
477 pharmacological disruption of either D2-MSNs or D1-MSNs increased response times, with
478 pharmacological D2 or D1 blockade shifting MSN dynamics and degrading temporal decoding.
479 Collectively, our data provide insight into how the striatum encodes cognitive information,
480 which could be highly relevant for human diseases that disrupt the striatum and for next-
481 generation neuromodulation that targets the basal ganglia to avoid cognitive side effects or to
482 treat cognitive dysfunction.
483

Methods and Materials

Rodents. All procedures were approved by the Institutional Animal Care and Use Committee (IACUC) at the University of Iowa, and all experimental methods were performed in accordance with applicable guidelines and regulations (Protocol #0062039). We used five cohorts of mice, summarized in Table 1: 1) 30 wild-type C57BL/6J mice (17 female) for behavioral experiments (Fig 1), 2) 4 *Drd2-cre*+ mice derived from Gensat strain ER44 (2 female) and 5 *Drd1-cre*+ mice derived from Gensat strain EY262 (2 female) for optogenetic tagging and neuronal ensemble recordings in Fig 2-3; 3) 10 *Drd2-cre*+ (5 female), and 6 *Drd1-cre*+ mice (3 female) for optogenetic inhibition with 5 *Drd2-cre*+ and 5 *Drd1-cre*+ controls (Fig 5) and 4) 10 wild-type mice for behavioral pharmacology (Fig 6), and 5) 11 mice (4 C57BL/6J (2 female), 5 *Drd2-cre*+ mice (2 female), and 2 *Drd1-cre*+ mice (0 female)) for combined behavioral pharmacology and neuronal ensemble recording (Fig 6-7) (Table 1). Our recent work shows that D2-blockade and D1-blockade have similar effects in both sexes (Stutt et al., 2023).

Interval timing switch task. We used a mouse-optimized operant interval timing task described in detail previously (Balci et al., 2008; Bruce et al., 2021; Stutt et al., 2023; Tosun et al., 2016; Weber et al., 2023). Briefly, mice were trained in sound-attenuating operant chambers, with two front nosepokes flanking either side of a food hopper on the front wall, and a third nosepoke located at the center of the back wall. The chamber was positioned below an 8-kHz, 72-dB speaker (Fig 1A; MedAssociates, St. Albans, VT). Mice were 85% food restricted and motivated with 20 mg sucrose pellets (Bio-Serv, Flemington, NJ). Mice were initially trained to receive rewards during fixed ratio nosepoke response trials. Nosepoke entry and exit were captured by infrared beams. After shaping, mice were trained in the “switch” interval timing task. Mice self-

506 initiated trials at the back nosepoke, after which a tone and nosepoke lights were illuminated
507 simultaneously. Cues were identical on all trial types and lasted the entire trial duration (6 or
508 18s). On 50% of trials, mice were rewarded for a nosepoke after 6 seconds at the designated
509 'first' front nosepoke (counterbalanced across animals to be left or right of the food hopper;
510 included as a regressor in neuronal analyses); these trials were not analyzed. On the remaining
511 50% of trials, mice were rewarded for nosepoking first at the 'first nosepoke and then switching
512 responses to the 'second' nosepoke (reward given only after responding at the 'second' nosepoke
513 after 18s). Switch *response time* was defined as switch from the first to the second nosepoke and
514 is represented by the time mice exited the first nosepoke prior to entering the second nosepoke.
515 Critically, switch responses are a time-based decision guided by temporal control of action
516 because mice switch nosepokes only if nosepokes at the first location did not receive reward
517 after 6 seconds. That is, mice estimate if more than 6 seconds have elapsed without receiving
518 reward to decide to switch responses. Mice learn this task quickly (3-4 weeks), and error trials in
519 which an animal nosepokes in the wrong order or does not nosepoke are relatively rare and
520 discarded. Consequently, we focused on these switch response times as the key metric for
521 temporal control of action. Switch *response duration* was defined as the time between first
522 nosepoke entry and exit for the switch responses only. Switch *traversal time* was defined as the
523 duration between first nosepoke exit and second nosepoke entry. Trials were self-initiated, but
524 there was a intertrial interval with a geometric mean of 30 seconds between trials.

525 ***Surgical and histological procedures.*** Surgical procedures were identical to methods described
526 previously (Bruce et al., 2021). Briefly, mice were anesthetized using inhaled 4% isoflurane and
527 surgical levels of anesthesia were maintained at 1-2% for the duration of the surgery.
528 Craniotomies were drilled above bilateral dorsal striatal anatomical targets, and optogenetic

529 viruses (AAV5-DIO-eNHPR2.0 (halorhodopsin), AAV5-DIO-ChR2(H134R)-mcherry (ChR), or
530 AAV5-DIO-cherry (control) from the University of North Carolina Viral Vector Core) were
531 injected (0.5 uL of virus, +0.9, ML +/-1.3, DV –2.7). Either fiber optics (Doric Lenses, Montreal
532 Quebec; AP +0.9, ML +/-1.3, DV –2.5) or 4 x 4 electrode or optrode arrays (AP +0.4, ML -1.4,
533 DV -2.7 on the left side only; Microprobes, Gaithersburg, MD) were positioned in the dorsal
534 striatum. Holes were drilled to insert skull screws to anchor headcap assemblies and/or ground
535 electrode arrays and then sealed with cyanoacrylate ("SloZap," Pacer Technologies, Rancho
536 Cucamonga, CA), accelerated by "ZipKicker" (Pacer Technologies) and methyl methacrylate
537 (AM Systems, Port Angeles, WA). Following postoperative recovery, mice were trained on the
538 switch task and acclimated to experimental procedures prior to undergoing experimental
539 sessions.

540 ***Optogenetics.*** We leveraged cell-type-specific optogenetics to manipulate D2-MSNs and D1-
541 MSNs in D2- or D1-cre mice. In animals injected with optogenetic viruses, optical inhibition was
542 delivered via bilateral patch cables for the entire trial duration of 18 seconds via 589-nm laser
543 light at 12 mW power on 50% of randomly assigned trials. We did not stimulate for epochs less
544 than the interval because we did not want to introduce a cue during the interval. For optogenetic
545 tagging, putative D1- and D2-MSNs were optically identified via 473-nm photostimulation.
546 Units with mean post-stimulation spike latencies of ≤5 milliseconds and a stimulated-to-
547 unstimulated waveform correlation ratio of >0.9 were classified as putative D2+ or D1+
548 neurons(Ryan et al., 2018; Shin et al., 2018).

549 ***Behavioral pharmacology procedures.*** C57BL/6J mice were injected intraperitoneally (IP) 20-
550 40 minutes before interval timing trials with either SCH23390 ($C_{17}H_{18}ClNO$; D1 antagonist),

551 sulpiride ($C_{15}H_{23}N_3O_4S$; D2 antagonist), or isotonic saline. The sulpiride dosage was 12.5 mg/kg,
552 0.01 mL/g, and the SCH23390 was administered at a dosage of 0.05 mg/kg, 0.01 mL/g.
553 Behavioral performance was compared with interval timing behavior on the prior day when
554 isotonic saline was injected IP.

555 ***Electrophysiology.*** Single-unit recordings were made using a multi-electrode recording system
556 (Open Ephys, Atlanta, GA). After the experiments, Plexon Offline Sorter (Plexon, Dallas, TX),
557 was used to remove artifacts. Principal component analysis (PCA) and waveform shape were
558 used for spike sorting. Single units were defined as those 1) having a consistent waveform shape,
559 2) being a separable cluster in PCA space, and 3) having a consistent refractory period of at least
560 2 milliseconds in interspike interval histograms. Spike activity was analyzed for all cells that
561 fired between 0.5 Hz and 20 Hz over the entire behavioral session. Putative MSNs were further
562 separated from striatal fast-spiking interneurons (FSIs) based on hierarchical clustering of the
563 waveform peak-to-trough ratio and the half-peak width (*fitgmdist* and *cluster.m*; Fig S2; Berke,
564 2011). We calculated kernel density estimates of firing rates across the interval (-4 seconds
565 before trial start to 22 seconds after trial start) binned at 0.1 seconds, with a bandwidth of 1. We
566 used PCA to identify data-driven patterns of z-scored neuronal activity, as in our past
567 work(Bruce et al., 2021; Emmons et al., 2017; Kim et al., 2017a). Average plots were shown
568 with Gaussian smoothing for plotting purposes only.

569 ***Immunohistochemistry.*** Following completion of experiments, mice were transcardially
570 perfused with ice-cold 1x phosphate-buffered saline (PBS) and 4% paraformaldehyde (PFA)
571 after anesthesia using ketamine (100 mg/kg IP) and xylazine (10 mg/kg IP). Brains were then
572 fixed in solutions of 4% PFA and 30% sucrose prior to being cryosectioned on a freezing

573 microtome. Sections were stained for tyrosine hydroxylase with primary antibodies for >12
574 hours (rabbit anti-TH; Millipore MAB152; 1:1000) at 4° C. Sections were subsequently
575 visualized with Alexa Fluor fluorescent secondary antibodies (goat anti-rabbit IgG Alexa 519;
576 Thermo Fisher Scientific; 1:1,000) matched to host primary by incubating 2 hours at room
577 temperature. Histological reconstruction was completed using postmortem analysis of electrode
578 placement by slide-scanning microscopy on an Olympus VS120 microscope (Olympus, Center
579 Valley, PA; Fig S2&S4).

580 ***Trial-by-trial GLMs.*** To measure time-related ramping, we used trial-by-trial generalized linear
581 models (GLMs) at the individual neuron level in which the response variable was firing rate
582 binned at 0.1 seconds and the predictor variable was time in the interval or nosepoke
583 rate(Shimazaki and Shinomoto, 2007). For each neuron, it's time-related "ramping" slope was
584 derived from the GLM fit of firing rate vs time in the interval, for all trials per neuron. All GLMs
585 were run at a trial-by-trial level to avoid effects of trial averaging (Latimer et al., 2015) as in our
586 past work (Bruce et al., 2021; Emmons et al., 2017; Kim et al., 2017b).

587 ***Machine-learning analyses****:* We used feedforward neural network classifier (*fitcnet* in Matlab)
588 to predict response times. Response times were divided into tertiles and then coded as a discrete
589 class variable. Predictors were constructed from trial-by-trial kernel density estimates of firing
590 rates between 0 and 18 seconds using a bin size of 0.1 s and a bandwidth of 1 from all MSNs
591 within a single interval-timing session. We used layer sizes of 35, 20, and 10 using leave-one-out
592 validation. Classifier performance was quantified by accuracy of the confusion matrix for all
593 response-time tertiles.

To predict time, we used a naïve Bayesian classifier to evaluate neuronal ensemble decoding as in our past work(Emmons et al., 2017; Kim et al., 2017a). Only data from neurons with more than 20 trials was included. To preclude edge effects that might bias classifier performance, we included data from 6 seconds prior to the trial start and 6 seconds after the end of the interval. We used leave-one-out cross-validation to predict an objective time from the firing rate within a trial. Classifier performance was quantified by computing the R^2 of objective time vs predicted time, only for bins during the interval (0-6, 6-12, and 12-18 seconds; see Fig 7). Classifier performance was compared using time-shuffled firing rates via a Wilcoxon signed rank test.

Modeling. We constructed a four-parameter drift-diffusion model (see Equations 1-3 in Results) and used it to simulate response times compatible with mice behavioral data. The model was implemented in MATLAB, starting from initial value b and with discrete computer simulation steps $x_{new} = x_{old} + (F - x_{old})D\Delta t + \sigma\sqrt{\Delta t}N(0,1)$. Here $N(0,1)$ represents random values generated from the standardized Gaussian distribution (mean = 0 and standard deviation = 1). The integration timestep was taken $\Delta t = 0.1$ to be like the 0.1-second bin size used in the analysis of firing rate data. For each numerical simulation, the "response time" was defined as the time t^* when variable x first reached the threshold value $T = F(1 - b/4) + (1 - F)b/4$. For each condition, we ran 500 simulations of the model (up to 25 seconds per trial) and recorded the response times. Examples of firing rate x dynamics are shown in Fig 4A-B. We observed that the distributions of interval timing response times could be fit by a gamma probability distribution function $PDF(x) = \frac{\beta^\alpha}{\Gamma(\alpha)}\, x^{\alpha-1}\, e^{-\beta x}$ with shape α and rate β (see Fig S6 and Table S2).

615 ***Statistics.*** All data and statistical approaches were reviewed by the Biostatistics, Epidemiology,
616 and Research Design Core (BERD) at the Institute for Clinical and Translational Sciences
617 (ICTS) at the University of Iowa. All code and data are made available at
618 http://narayanan.lab.uiowa.edu/article/datasets. We used the median to measure central tendency
619 and the interquartile range to measure spread. We used Wilcoxon nonparametric tests to compare
620 behavior between experimental conditions and Cohen's *d* to calculate effect size. Analyses of
621 putative single-unit activity and basic physiological properties were carried out using custom
622 routines for MATLAB. To analyze neuronal activity, we used linear-mixed effects models (*lmer*
623 in R) to account for effects across individual mice, and linear models (*lm* in R) to account for
624 effects of sex and which direction mice were switching (i.e., mice switching left-to-right or right-
625 to-left). Post-hoc comparisons were performed for pharmacology sessions using *emmeans* in R.

626

Data Availability

All raw data are available at http://narayanan.lab.uiowa.edu/article/datasets.

Code Availability

All code is available at http://narayanan.lab.uiowa.edu/article/datasets.

Acknowledgements

This work was funded by NIMH R01MH116043 to NSN. We thank Bernardo Sabatini for detailed feedback on our manuscript.

Author Contributions

RAB, MAW, and NN designed the experiments. RAB, MAW, ASB, RV, CJ, and HRS performed all experiments and collected data. The data was analyzed by RAB, MAW, ASB, HRS, YK, RC, and NN. RC developed the computational model. RAB, MAW, ASB, KS, RC, and NN wrote the manuscript, and all authors reviewed and revised the manuscript.

Experiment	*Figure*	*Cohort*	*Mice*	*Neurons*
Interval timing behavior	Fig 1B-C	1	30 wild-type mice	~
Optogenetic Tagging of D2-MSNs	Fig 2-3	2	4 D2-Cre mice	32 D2-MSNs
Optogenetic Tagging of D1-MSNs	Fig 2-3		5 D1-Cre mice	41 D1-MSNs
Drift-diffusion models (DDM)	Fig 4A-D, Fig S6		~	~
Optogenetic Inhibition of D2-MSNs	Fig 5A-B	3	10 D2-Cre mice	~
Optogenetic Inhibition of D1-MSNs	Fig 5C-D		6 D1-Cre mice	~
Optogenetic D2-MSN controls	Fig S7		5 D2-Cre mice	~
Optogenetic D1-MSN controls	Fig S7		5 D1-Cre mice	~
Pharmacological D2 blockade	Fig 5E-F	4	10 wild-type mice	~
Pharmacological D1 blockade	Fig 5G-H		“	~
MSN ensemble recording - saline	Fig 6-7	5	4 wild-type mice	158 MSNs
MSN ensembles – D2 blockade	Fig 6-7		5 D2-cre mice, and	167 MSNs
MSN ensembles – D1 blockade	Fig 6-7		2 D1-cre mice	144 MSNs

Table 1: Summary of mice and MSNs

Supplementary Information

Condition	***Source***	***α***	***β***	
D2-MSNs Laser Off	Empirical Data	6.03	0.67	Fig S6A
D2-MSNs Laser Off	Model	6.08	0.69	Fig S6E
D2-MSNs Inhibited	Empirical Data	7.62	0.78	Fig S6B
D2-MSNs Inhibited	Model	7.67	0.79	Fig S6F
D1-MSNs Laser Off	Empirical Data	5.87	0.68	Fig S6C
D1-MSNs Laser Off	Model	5.89	0.69	Fig S6G
D1-MSNs Inhibited	Empirical Data	7.13	0.70	Fig S6D
D1-MSNs Inhibited	Model	7.31	0.72	Fig S6H

Table S2: Gamma distribution parameters

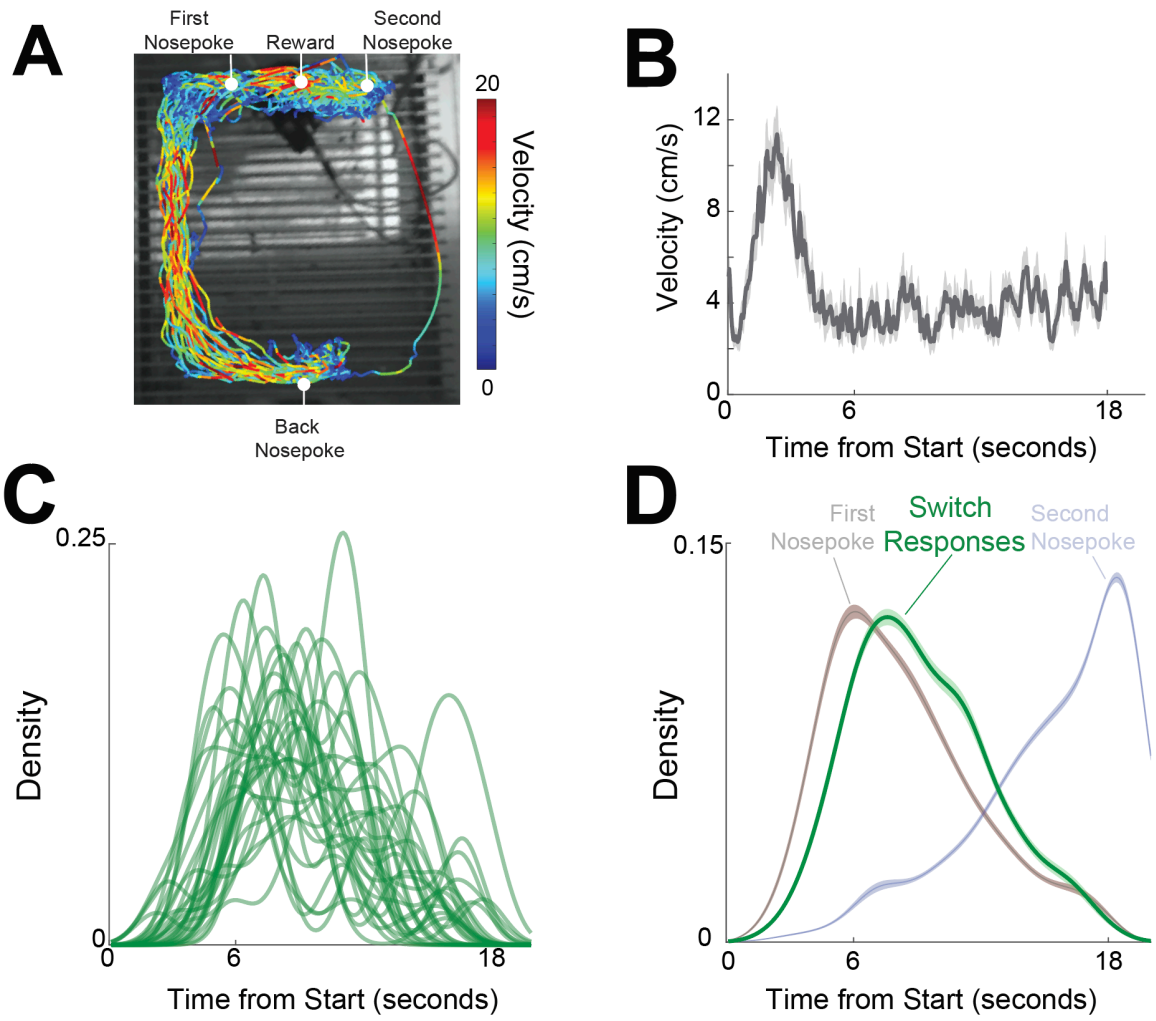

Figure S1: A) DeepLabCut tracking of position during the interval timing. B) Mice moved quickly after trial start and then velocity was relatively constant throughout the trial. C) Probability distribution of switch responses from 30 animals; each line is the average for one animal. D) Probability distribution of first nosepokes (grey), switch responses when mice depart the first nosepoke (in green; average of panel C), and second nosepokes (blue). Shaded bars represent standard error; data from the same 30 mice as from Figure 1B-C.

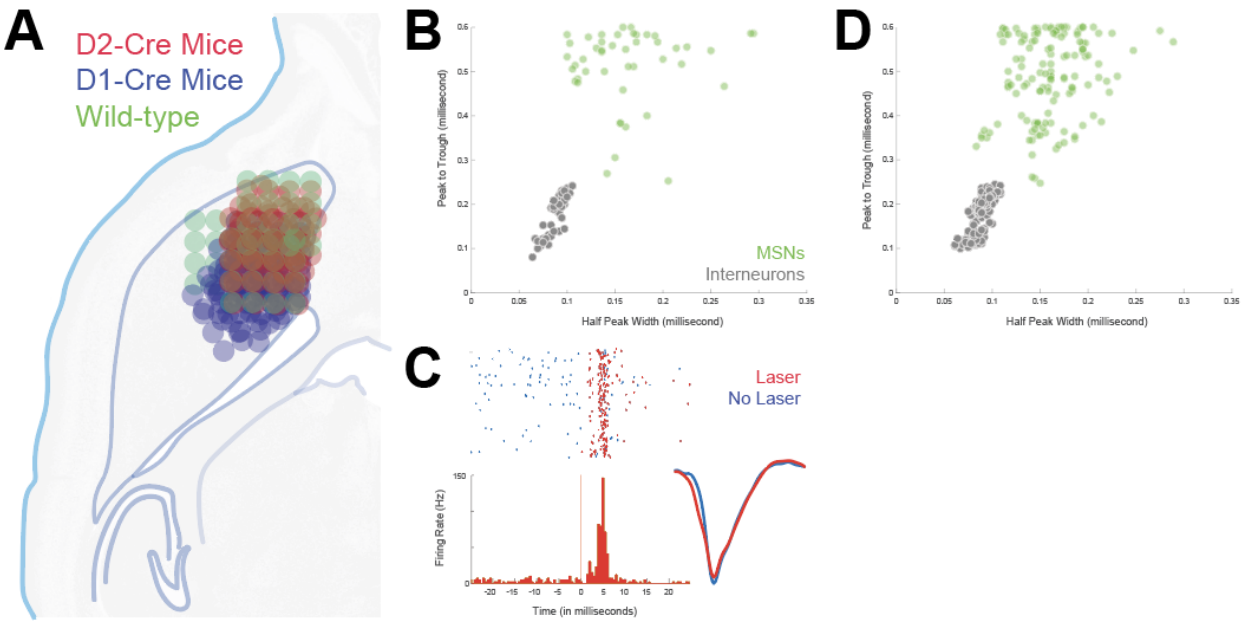

Figure S2: A) Recording locations in the dorsomedial striatum. Electrode reconstructions for D2-Cre (red), D1-Cre (blue), and wild-type mice (green). Only the left striatum was implanted with electrodes in all animals. B) MSN classification by waveform criteria for sessions with optogenetic tagging. C) Example of an optogenetically tagged MSN. This neuron expresses ChR2, and on trials when the 473 nm laser was pulsed (thin red line), this neuron fired action potentials within 5 milliseconds. Inset on bottom right – waveforms from laser trials (red) and trials without laser (blue). Across 73 tagged neurons, waveform correlation coefficients for laser trials vs. trials without laser was r = 0.97 (0.92-0.99). D) MSN classification by waveform criteria for pharmacology sessions.

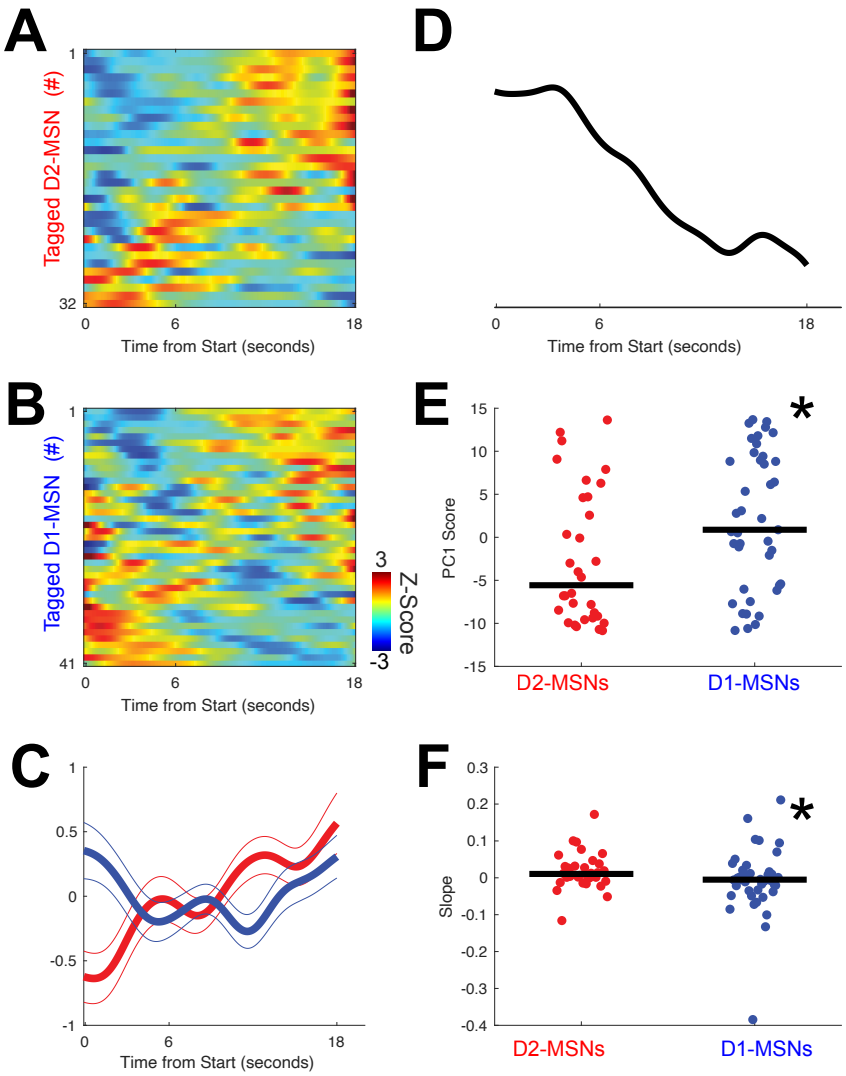

Figure S3: D2- and D1-MSN activity over the whole 18-second interval. A) Peri-event time histograms from D2-MSNs and B) from D1-MSNs over the whole interval. C) We noticed that on average, D2-MSNs tended to ramp up (red), whereas D1-MSNs tended to ramp down (blue). D) Principal component analysis revealed that PC1 exhibited time-dependent ramping over the whole 18-second interval. This component explained ~45% of variance across tagged MSN ensembles. E) Over the whole interval, differences between D2-MSNs and D1-MSNs were captured in PC1, which indicates opposing time-dependent ramping (rank sum $p = 0.02$). F)

688 These differences were also captured via differences in a linear slope of firing rate vs time over
689 the whole 18-second interval, with D1-MSNs having a more negative slope (rank sum $p = 0.03$).
690 Data from 32 tagged D2-MSNs in 4 D2-Cre mice and 41 tagged D1-MSNs in 5 D1-Cre mice
691 (see Figs. 1).
692

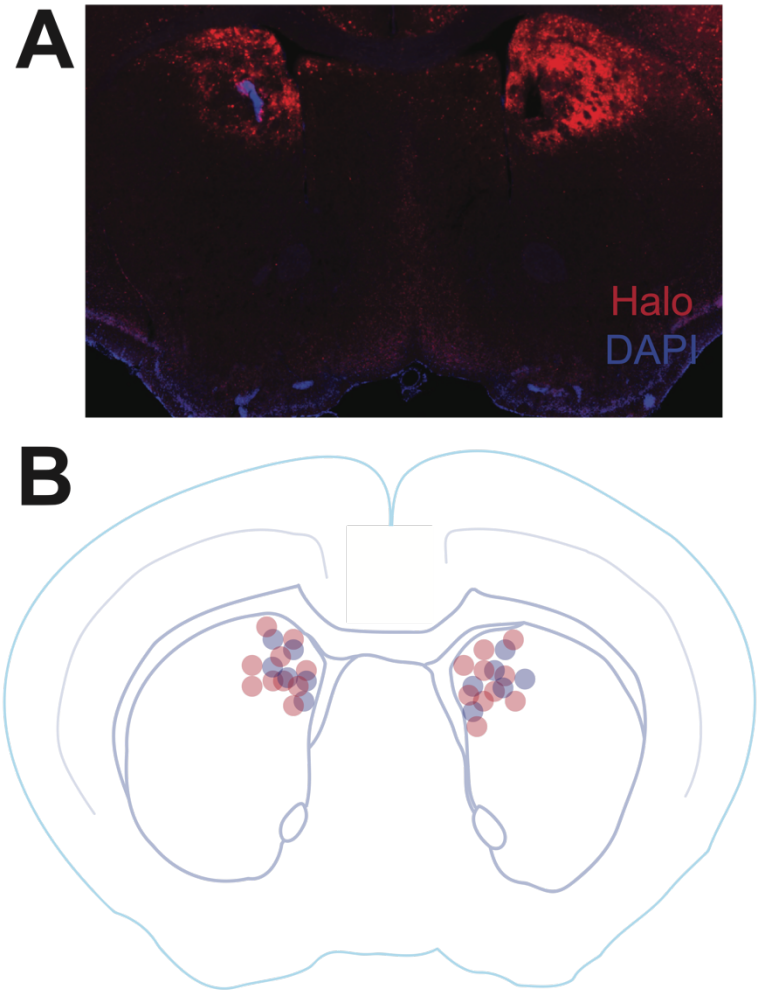

Figure S4: Fiber optic locations from A) an opsin-expressing mouse with mCherry-tagged halorhodopsin and bilateral fiber optics, and B) across 10 D2-Cre mice (red) and 6 D1-cre mice (blue) with fiber optics.

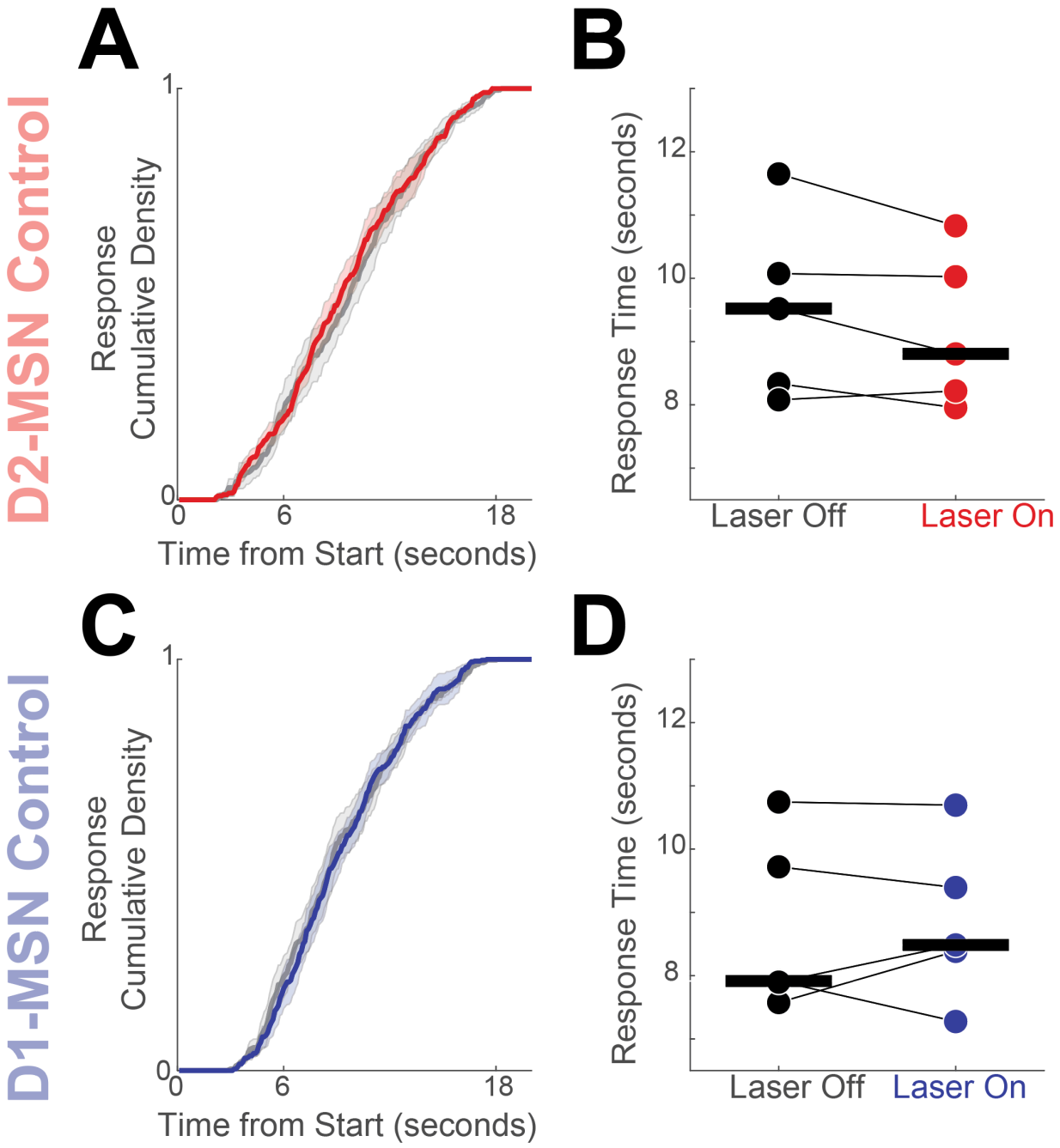

Figure S5: Experiments in D2-Cre mice injected with virus without opsins did not reliably affect A) cumulative density functions (CDFs) or B) response times (signed rank $p = 0.44$). Experiments in D1-Cre mice expressing virus without opsins did not reliably affect C) CDFs or D) response times (signed rank $p = 0.81$).

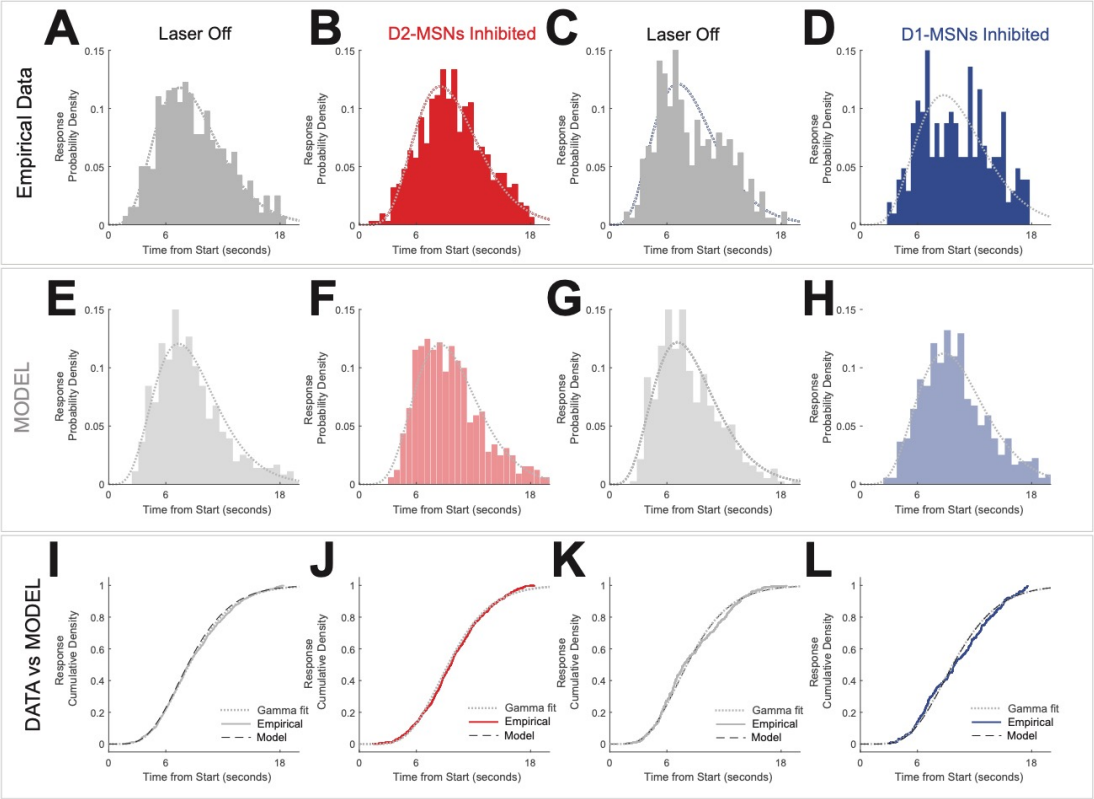

Figure S6: Model details. Histograms of behavioral data from D2-Cre mice with A) Laser Off and B) D2-MSN inhibition (red). Data from D1-Cre mice with C) Laser Off and with D) D1-MSN inhibition (blue). E-H) model predictions. I-J) Comparisons of empirical data vs model. All panels: fits for the gamma distribution with dotted circles; see Table S2 for the parameter values defining each gamma distribution. Behavioral data: from 10 D2-Cre mice and 6 D1-mice from Fig 1A-D. Model data: from numerical simulations of the DDM model shown in Fig 2.

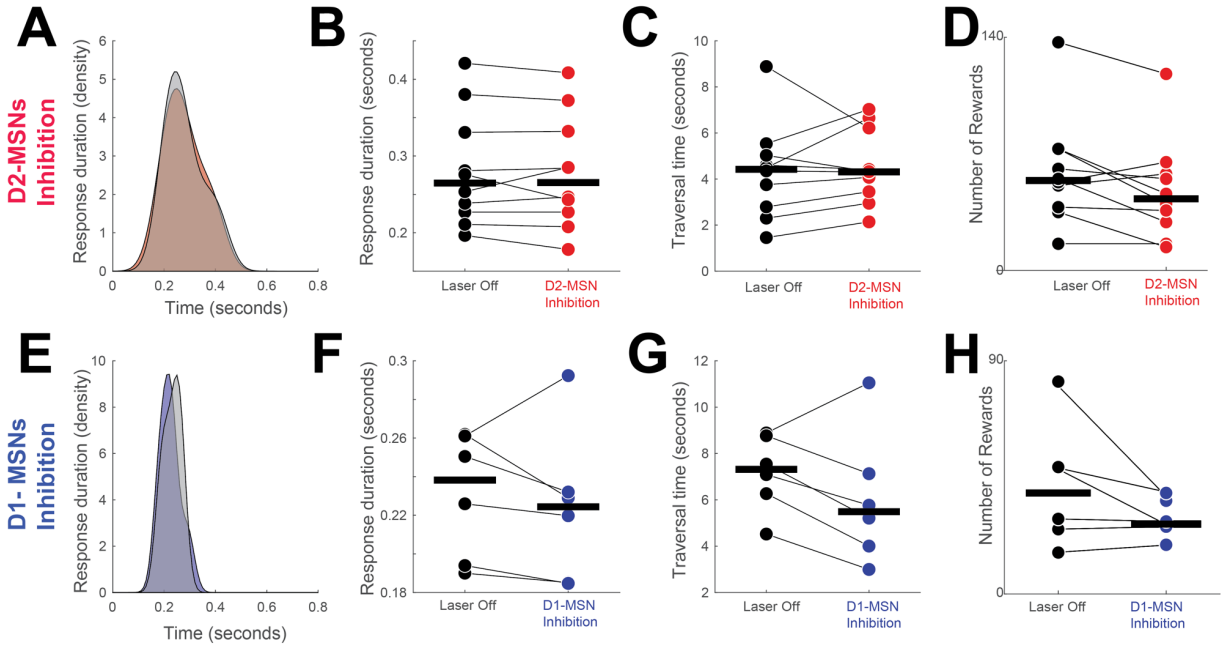

Figure S7: Optogenetically inhibiting D2-MSNs or D1-MSNs does not affect task-specific motor control. We measured nosepoke duration (time of nosepoke entry to exit) on switch responses. During interval timing there was no effect of optogenetic inhibition (red) of dorsomedial striatal D2-MSNs on A-B) nosepoke duration or C) the traversal time between the first and second nosepokes. There was also no effect of optogenetic inhibition (blue) of dorsomedial striatal D1-MSNs on response duration (D-E) or F) switch traversal time. Data from the same 10 D2-Cre mice and 6 D1-Cre mice, as in Fig 5. Horizontal black lines in B,C,E, and F represent group medians.

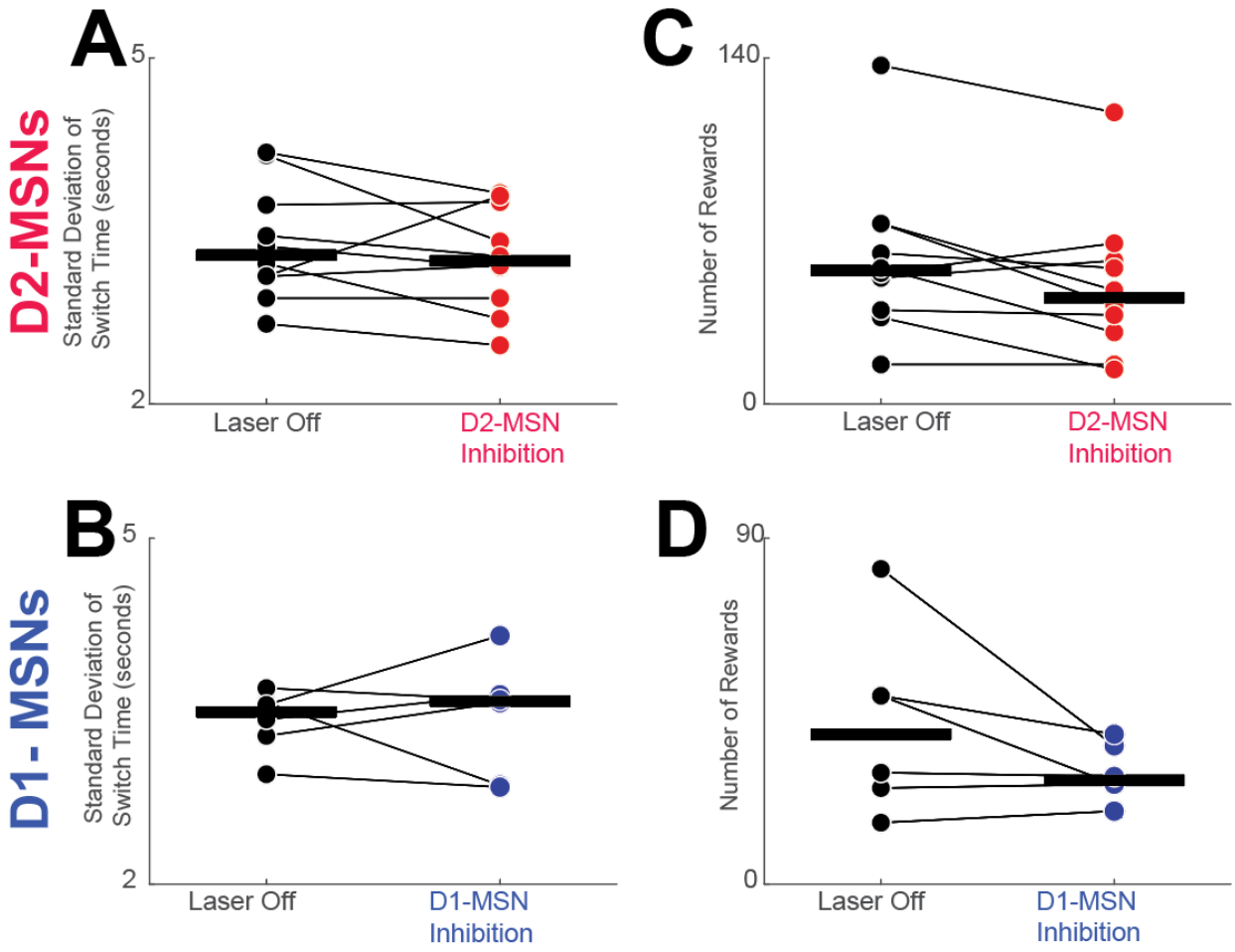

Figure S8: A) Standard deviation of interval timing performance for D2-MSN inhibition sessions (signed rank test, $p = 0.19$) and B) D1-MSN inhibition sessions ($p = 0.84$), and the number of total rewards for C) D2-MSN inhibition sessions ($p = 0.07$) and d) D1-MSN inhibition sessions ($p = 0.24$). Data from 10 D2-Cre mice and 6 D1-Cre mice as in Fig 5.

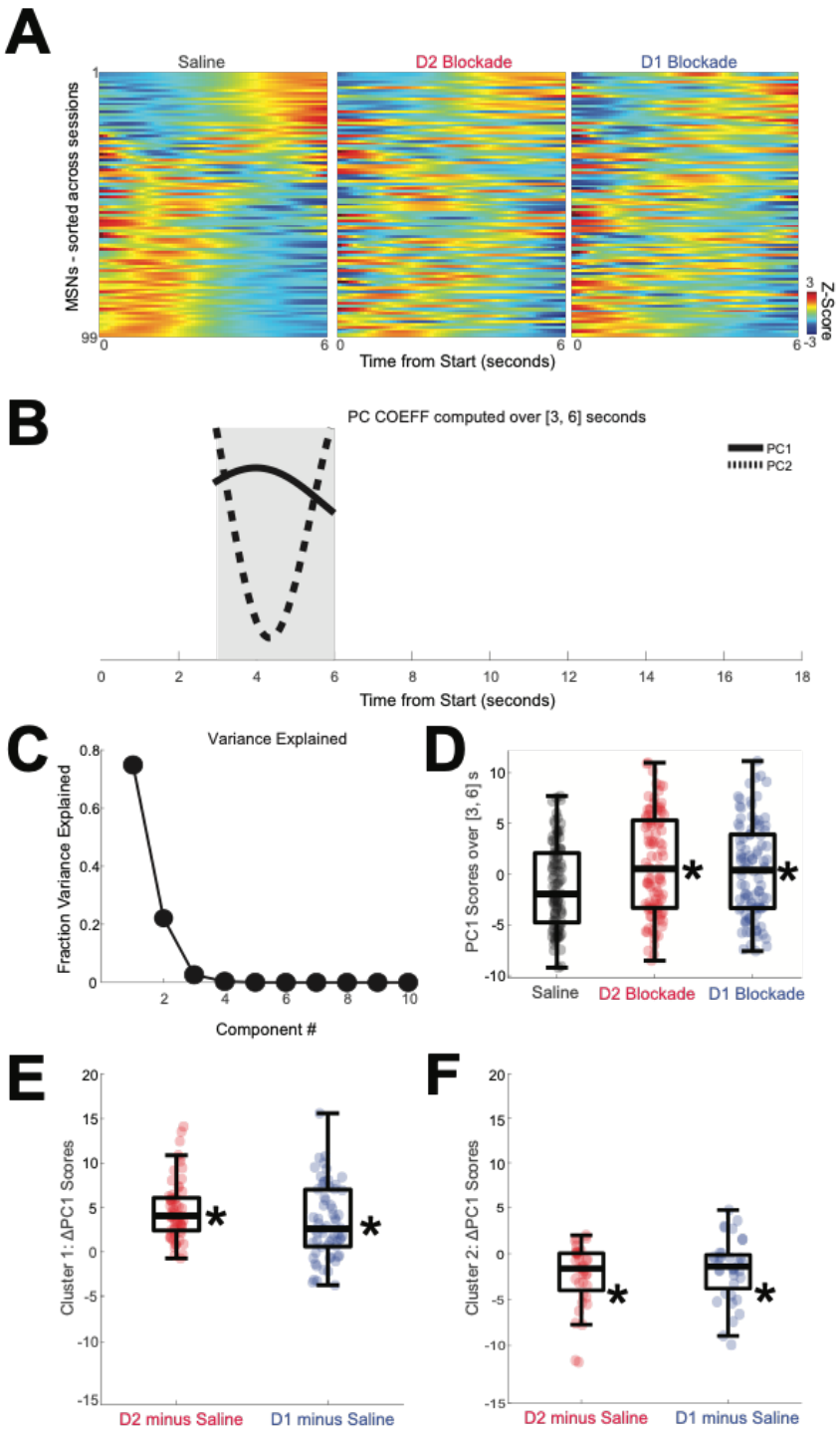

Figure S9: A) We sorted and identified the same 99 MSNs across saline sessions and sessions with D2 blockade or D1 blockade. Each row is a z-scored peri-event time histogram of MSN

activity for all trials during interval timing. Each row is the same neuron identified by waveform and interspike-intervals across saline, D2 blockade, and D1 blockade sessions. B) We further explored early-interval dynamics by PCA. The matched sorting across sessions enabled paired signed rank analyses. C) The first component (PC1) explained 75% of variance among MSN ensemble dynamics between 3-6 seconds that showed maximal differences between sessions. D) As with dynamics between 0-6 seconds, PC1 was shifted relative to saline for D2 blockade (signed rank $p = 0.000007$) and D1 blockade (signed rank $p = 0.002$). We identified two clusters based on PC1, with cluster 1 (E) loading positively on PC1, and cluster 2 (F) loading negatively on PC1. For cluster 1 in (E), PCs were distinct from saline for D2 blockade (signed rank $p = 3\text{x}10^{-12}$) and for D1 blockade (signed rank $p = 10^{-7}$). For cluster 2 in panel (F), PC1 changes were also distinct for saline for D2 blockade (signed rank $p = 0.00008$) and for D1 blockade (signed rank $p = 0.002$). Data from the same mice as in Fig 6.

REFERENCES

Albin RL, Young AB, Penney JB. 1989. The functional anatomy of basal ganglia disorders. *Trends Neurosci* **12**:366–375. doi:10.1016/0166-2236(89)90074-X

Alexander GE, Crutcher MD. 1990. Functional architecture of basal ganglia circuits: neural substrates of parallel processing. *Trends Neurosci* **13**:266–271. doi:10.1016/0166-2236(90)90107-L

Andreasen NC. 1999. Understanding the causes of schizophrenia. *N Engl J Med* **340**:645–647. doi:10.1056/NEJM199902253400811

Averbeck BB, Lehman J, Jacobson M, Haber SN. 2014. Estimates of projection overlap and zones of convergence within frontal-striatal circuits. *J Neurosci* **34**:9497–9505.

Balci F, Gallistel CR. 2006. Cross-domain transfer of quantitative discriminations: Is it all a matter of proportion? *Psychon Bull Rev* **13**:636–642. doi:10.3758/BF03193974

Balci F, Papachristos EB, Gallistel CR, Brunner D, Gibson J, Shumyatsky GP. 2008. Interval timing in genetically modified mice: a simple paradigm. *Genes Brain Behav* **7**:373–384. doi:10.1111/j.1601-183X.2007.00348.x

Berke JD. 2011. Functional properties of striatal fast-spiking interneurons. *Front Syst Neurosci* **5**:45.

Bruce RA, Weber MA, Volkman RA, Oya M, Emmons EB, Kim Y, Narayanan NS. 2021. Experience-related enhancements in striatal temporal encoding. *Eur J Neurosci* **54**:5063–5074. doi:10.1111/ejn.15344

Cruz BF, Guiomar G, Soares S, Motiwala A, Machens CK, Paton JJ. 2022. Action suppression reveals opponent parallel control via striatal circuits. *Nature* **607**:521–526. doi:10.1038/s41586-022-04894-9

Cui G, Jun SB, Jin X, Pham MD, Vogel SS, Lovinger DM, Costa RM. 2013. Concurrent activation of striatal direct and indirect pathways during action initiation. *Nature* **494**:238–242. doi:10.1038/nature11846

De Corte BJ, Wagner LM, Matell MS, Narayanan NS. 2019. Striatal dopamine and the temporal control of behavior. *Behav Brain Res* **356**:375–379. doi:10.1016/j.bbr.2018.08.030

Drew MR, Fairhurst S, Malapani C, Horvitz JC, Balsam PD. 2003. Effects of dopamine antagonists on the timing of two intervals. *Pharmacol Biochem Behav* **75**:9–15.

Drew MR, Simpson EH, Kellendonk C, Herzberg WG, Lipatova O, Fairhurst S, Kandel ER, Malapani C, Balsam PD. 2007. Transient Overexpression of Striatal D2 Receptors Impairs Operant Motivation and Interval Timing. *J Neurosci* **27**:7731–7739. doi:10.1523/JNEUROSCI.1736-07.2007

Emmons EB, De Corte BJ, Kim Y, Parker KL, Matell MS, Narayanan NS. 2017. Rodent medial frontal control of temporal processing in the dorsomedial striatum. *J Neurosci* **37**:8718–8733.

Emmons EB, Tunes-Chiuffa G, Choi J, Bruce RA, Weber MA, Kim Y, Narayanan NS. 2020. Temporal Learning Among Prefrontal and Striatal Ensembles. *Cereb Cortex Commun* **1**. doi:10.1093/texcom/tgaa058

Gerfen CR. 1984. The neostriatal mosaic: compartmentalization of corticostriatal input and striatonigral output systems. *Nature* **311**:461–464. doi:10.1038/311461a0

Gouvea TS, Monteiro T, Motiwala A, Soares S, Machens C, Paton JJ. 2015. Striatal dynamics explain duration judgments. *eLife* **4**. doi:10.7554/eLife.11386

Graybiel AM. 1997. The Basal Ganglia and Cognitive Pattern Generators. *Schizophr Bull* **23**:459–469. doi:10.1093/schbul/23.3.459

Gür E, Duyan YA, Arkan S, Karson A, Balcı F. 2020. Interval timing deficits and their neurobiological correlates in aging mice. *Neurobiol Aging* **90**:33–42. doi:10.1016/j.neurobiolaging.2020.02.021

Gür E, Fertan E, Alkins K, Wong AA, Brown RE, Balcı F. 2019. Interval timing is disrupted in female 5xFAD mice: An indication of altered memory processes. *J Neurosci Res* **97**:817–827. doi:https://doi.org/10.1002/jnr.24418

Hinton SC, Paulsen JS, Hoffmann RG, Reynolds NC, Zimbelman JL, Rao SM. 2007. Motor timing variability increases in preclinical Huntington's disease patients as estimated onset of motor symptoms approaches. *J Int Neuropsychol Soc* **13**:539–543. doi:10.1017/S1355617707070671

Kim Y-C, Han S-W, Alberico SL, Ruggiero RN, De Corte B, Chen K-H, Narayanan NS. 2017a. Optogenetic Stimulation of Frontal D1 Neurons Compensates for Impaired Temporal Control of Action in Dopamine-Depleted Mice. *Curr Biol CB* **27**:39–47. doi:10.1016/j.cub.2016.11.029

Kim Y-C, Han S-W, Alberico SL, Ruggiero RN, De Corte B, Chen K-H, Narayanan NS. 2017b. Optogenetic stimulation of frontal D1 neurons compensates for impaired temporal control of action in dopamine-depleted mice. *Curr Biol* **27**:39–47.

Kravitz AV, Freeze BS, Parker PR, Kay K, Thwin MT, Deisseroth K, Kreitzer AC. 2010. Regulation of parkinsonian motor behaviours by optogenetic control of basal ganglia circuitry. *Nature* **466**:622–626.

Kreitzer AC. 2009. Physiology and Pharmacology of Striatal Neurons. *Annu Rev Neurosci* **32**:127–147. doi:10.1146/annurev.neuro.051508.135422

Larson T, Khandelwal V, Weber MA, Leidinger MR, Meyerholz DK, Narayanan NS, Zhang Q. 2022. Mice expressing P301S mutant human tau have deficits in interval timing. *Behav Brain Res* **432**:113967. doi:10.1016/j.bbr.2022.113967

Latimer KW, Yates JL, Meister ML, Huk AC, Pillow JW. 2015. Single-trial spike trains in parietal cortex reveal discrete steps during decision-making. *Science* **349**:184–187.

Matell MS, Meck WH. 2004. Cortico-striatal circuits and interval timing: coincidence detection of oscillatory processes. *Cogn Brain Res*, Neuroimaging of Interval Timing **21**:139–170. doi:10.1016/j.cogbrainres.2004.06.012

Matell MS, Meck WH, Nicolelis MAL. 2003. Interval timing and the encoding of signal duration by ensembles of cortical and striatal neurons. *Behav Neurosci* **117**:760–773. doi:10.1037/0735-7044.117.4.760

Meck WH. 2006. Neuroanatomical localization of an internal clock: A functional link between mesolimbic, nigrostriatal, and mesocortical dopaminergic systems. *Brain Res* **1109**:93–107. doi:10.1016/j.brainres.2006.06.031

Mello GBM, Soares S, Paton JJ. 2015. A Scalable Population Code for Time in the Striatum. *Curr Biol* **25**:1113–1122. doi:10.1016/j.cub.2015.02.036

Merchant H, de Lafuente V. 2014. Introduction to the neurobiology of interval timing. *Adv Exp Med Biol* **829**:1–13. doi:10.1007/978-1-4939-1782-2_1

Middleton FA, Strick PL. 2000. Basal ganglia and cerebellar loops: motor and cognitive circuits. *Brain Res Rev* **31**:236–250. doi:10.1016/S0165-0173(99)00040-5

Monteiro T, Rodrigues FS, Pexirra M, Cruz BF, Gonçalves AI, Rueda-Orozco PE, Paton JJ. 2023. Using temperature to analyze the neural basis of a time-based decision. *Nat Neurosci*. doi:10.1038/s41593-023-01378-5

845 Narayanan NS. 2016. Ramping activity is a cortical mechanism of temporal control of action.
846 *Curr Opin Behav Sci* **8**:226–230. doi:10.1016/j.cobeha.2016.02.017
847 Narayanan NS, Albin RL. 2022. Cognition in Parkinson's Disease, Progress in Brain Research.
848 Elsevier, Acad. Press.
849 Nguyen Q-A, Rinzel J, Curtu R. 2020. Buildup and bistability in auditory streaming as an
850 evidence accumulation process with saturation. *PLOS Comput Biol* **16**:e1008152.
851 doi:10.1371/journal.pcbi.1008152
852 Parker KL, Lamichhane D, Caetano MS, Narayanan NS. 2013. Executive dysfunction in
853 Parkinson's disease and timing deficits. *Front Integr Neurosci* **7**:75.
854 doi:10.3389/fnint.2013.00075
855 Paton JJ, Buonomano DV. 2018. The Neural Basis of Timing: Distributed Mechanisms for
856 Diverse Functions. *Neuron* **98**:687–705. doi:10.1016/j.neuron.2018.03.045
857 Robbe D. 2023. Lost in time: Relocating the perception of duration outside the brain. *Neurosci*
858 *Biobehav Rev* **153**:105312. doi:10.1016/j.neubiorev.2023.105312
859 Ryan MB, Bair-Marshall C, Nelson AB. 2018. Aberrant striatal activity in parkinsonism and
860 levodopa-induced dyskinesia. *Cell Rep* **23**:3438–3446.
861 Shepherd GMG. 2013. Corticostriatal connectivity and its role in disease. *Nat Rev Neurosci*
862 **14**:278–291. doi:10.1038/nrn3469
863 Shimazaki H, Shinomoto S. 2007. A Method for Selecting the Bin Size of a Time Histogram.
864 *Neural Comput* **19**:1503–1527. doi:10.1162/neco.2007.19.6.1503
865 Shin JH, Kim D, Jung MW. 2018. Differential coding of reward and movement information in
866 the dorsomedial striatal direct and indirect pathways. *Nat Commun* **9**:1–14.
867 Simen P, Balci F, de Souza L, Cohen JD, Holmes P. 2011. A model of interval timing by neural
868 integration. *J Neurosci Off J Soc Neurosci* **31**:9238–9253.
869 doi:10.1523/JNEUROSCI.3121-10.2011
870 Singh A, Cole RC, Espinoza AI, Evans A, Cao S, Cavanagh JF, Narayanan NS. 2021. Timing
871 variability and midfrontal ~4 Hz rhythms correlate with cognition in Parkinson's disease.
872 *NPJ Park Dis* **7**:14. doi:10.1038/s41531-021-00158-x
873 Stutt HR, Weber MA, Cole RC, Bova AS, Ding X, McMurrin MS, Narayanan NS. 2023. Sex
874 similarities and dopaminergic differences in interval timing. *Behavioral neuroscience (in*
875 *press)*
876 Tecuapetla F, Jin X, Lima SQ, Costa RM. 2016. Complementary Contributions of Striatal
877 Projection Pathways to Action Initiation and Execution. *Cell* **166**:703–715.
878 doi:10.1016/j.cell.2016.06.032
879 Toda K, Lusk NA, Watson GDR, Kim N, Lu D, Li HE, Meck WH, Yin HH. 2017. Nigrotectal
880 Stimulation Stops Interval Timing in Mice. *Curr Biol* **27**:3763-3770.e3.
881 doi:10.1016/j.cub.2017.11.003
882 Tosun T, Gur E, Balci F. 2016. Mice plan decision strategies based on previously learned time
883 intervals, locations, and probabilities. *Proc Natl Acad Sci U S A* **113**:787–792.
884 doi:10.1073/pnas.1518316113
885 Wang J, Narain D, Hosseini EA, Jazayeri M. 2018. Flexible timing by temporal scaling of
886 cortical responses. *Nat Neurosci* **21**:102. doi:10.1038/s41593-017-0028-6
887 Ward RD, Kellendonk C, Kandel ER, Balsam PD. 2011. Timing as a window on cognition in
888 schizophrenia. *Neuropharmacology*. doi:10.1016/j.neuropharm.2011.04.014
889 Weber MA, Sivakumar K, Tabakovic EE, Oya M, Aldridge GM, Zhang Q, Simmering JE,
890 Narayanan NS. 2023. Glycolysis-enhancing α1-adrenergic antagonists modify cognitive

symptoms related to Parkinson's disease. *Npj Park Dis* **9**:1–7. doi:10.1038/s41531-023-00477-1

Yun S, Yang B, Anair JD, Martin MM, Fleps SW, Pamukcu A, Yeh N-H, Contractor A, Kennedy A, Parker JG. 2023. Antipsychotic drug efficacy correlates with the modulation of D1 rather than D2 receptor-expressing striatal projection neurons. *Nat Neurosci* 1–12. doi:10.1038/s41593-023-01390-9